Report No. K-TRAN: KU-17-4 ▪ FINAL REPORT ▪ March 2021

Large Box Study on Granular Base Options for Portland Cement Concrete Pavements

Tanya N. Walkenbach, Ph.D.
Jie Han, Ph.D, P.E., F.ASCE
Robert L. Parsons, Ph.D., P.E.
Zexia Li

The University of Kansas

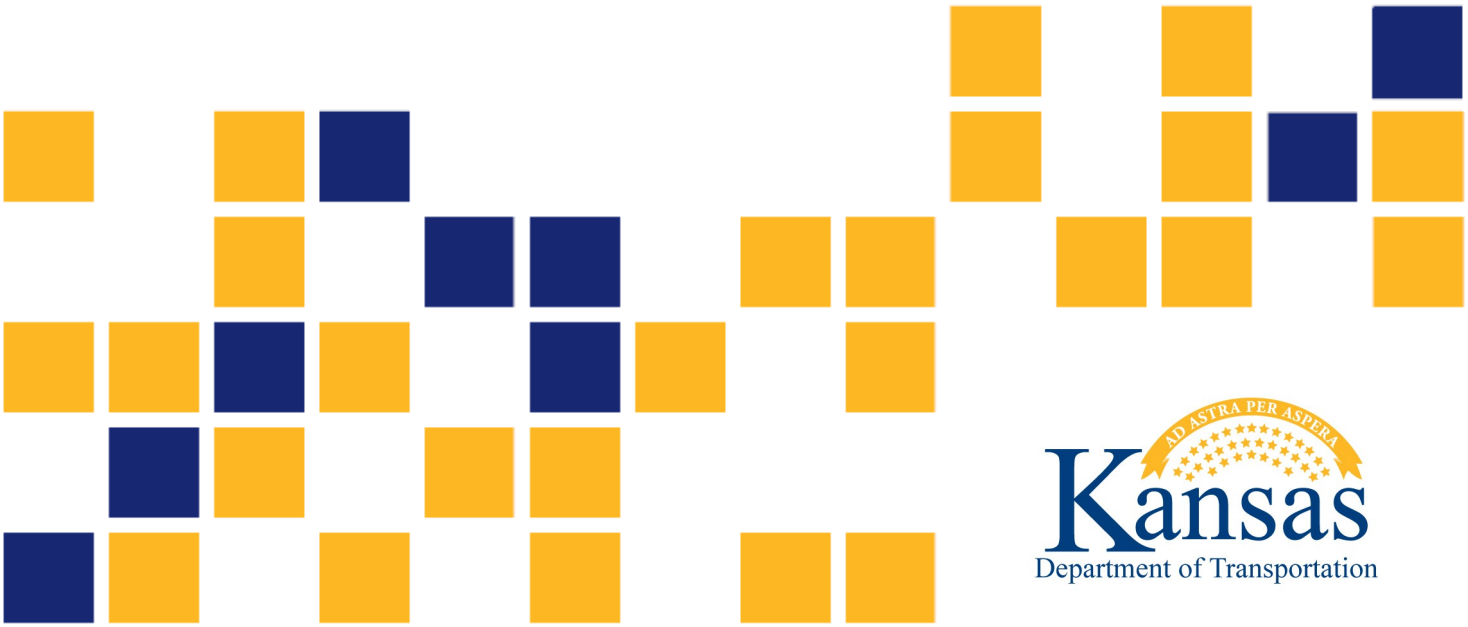

Kansas Department of Transportation

1 Report No. K-TRAN: KU-17-4	**2 Government Accession No.**	**3 Recipient Catalog No.**
4 Title and Subtitle Large Box Study on Granular Base Options for Portland Cement Concrete Pavements		**5 Report Date** March 2021 **6 Performing Organization Code**
7 Author(s) Tanya N. Walkenbach, Ph.D.; Jie Han, Ph.D., P.E., F.ASCE; Robert L. Parsons, Ph.D., P.E.; Zexia Li		**8 Performing Organization Report No.**
9 Performing Organization Name and Address The University of Kansas Department of Civil, Environmental & Architectural Engineering 1530 West 15th St Lawrence, Kansas 66045-7609		**10 Work Unit No. (TRAIS)** **11 Contract or Grant No.** C2092
12 Sponsoring Agency Name and Address Kansas Department of Transportation Bureau of Research 2300 SW Van Buren Topeka, Kansas 66611-1195		**13 Type of Report and Period Covered** Final Report July 2016–December 2019 **14 Sponsoring Agency Code** RE-0717-01

15 Supplementary Notes
For more information write to address in block 9.

16 Abstract

With the depletion of natural resources and limited funding for necessary pavement construction and rehabilitation, recycled concrete aggregate (RCA) and reclaimed asphalt pavement (RAP) are potential alternatives to the virgin granular base (VGB) typically used. The addition of geosynthetics at the interface of base course and subgrade can stabilize base course sections through separation, lateral restraint, and a tensioned membrane effect.

This large-scale box study focused on two different granular base options (VGB and RCA) with geosynthetic stabilization for concrete pavement applications. Unpaved road tests under cyclic loading were first conducted on these granular bases over weak subgrade to evaluate the benefits of three types of geosynthetics (nonwoven geotextile, woven geotextile, and triaxial geogrid) and replacement of VGB with RCA in the improved performance (permanent deformation and stress reduction) and properties (resilient modulus and modulus of subgrade reaction). The nonwoven geotextile was selected for three concrete paved roads with VGB and RCA over the same subgrade under cyclic loading. Displacement transducers and earth pressure cells were placed in the test sections to monitor resilient and permanent deformations on the section surface and vertical interface stresses between base course and subgrade.

For the unpaved test sections, the measured resilient and permanent deformations and the interface stress reduction were analyzed to evaluate the benefits of geosynthetics and replacement of VGB with RCA. The modified Burmister solution and the stress reduction method were used to back-calculate the resilient moduli (Mr) of the granular bases for all the test sections. Back-calculated resilient moduli were correlated with the accumulated permanent deformations to assess these methods. The American Association of State Highway and Transportation Officials (AASHTO, 1993) design chart was used to estimate the composite subgrade reaction moduli of the unpaved test sections based on the back-calculated resilient moduli (Mr) of the granular bases.

The three concrete paved sections and the benefits of the nonwoven geotextile and the replacement of VGB with RCA were evaluated in terms of their total and permanent displacements and base course-subgrade interface stresses. Based on the measured vertical displacements at the loaded corner, Westergaard's (1926) method was used to back-calculate the subgrade reaction moduli of these sections and estimate the tensile stresses in the concrete slabs. The back-calculated subgrade reaction moduli of these concrete paved sections were compared with those calculated based on the unpaved road sections.

The key findings of this study are: (1) geosynthetics were effective in reducing the permanent deformations of both VGB and RCA base courses over the weak subgrade in unpaved and concrete paved roads under cyclic loading; (2) RCA was stronger and stiffer than VGB and replacement of VGB with RCA reduced the permanent deformations in unpaved and concrete paved roads under cyclic loading; (3) the resilient modulus of the base course in an unpaved road section back-calculated by the modified Burmister solution with the mechanistic-empirical damage model was correlated well with the accumulated permanent deformation of the unpaved road section; (4) the modulus of subgrade reaction of a base over a subgrade estimated by the AASHTO design chart with the back-calculated resilient modulus of the base from an unpaved road test was similar to that back-calculated by the Westergaard solution based on the displacement at the loaded corner; (5) the accumulated permanent deformation of an unpaved or concrete paved section increased with the reduction of the subgrade reaction modulus in a semi-logarithmic relationship; and (6) geosynthetic stabilization and/or replacement of VGB with RCA increased the resilient modulus and the subgrade reaction modulus of a test section.

17 Key Words Reclaimed asphalt pavements, Concrete aggregates, Granular bases, Geosynthetics, Deformation		**18 Distribution Statement** No restrictions. This document is available to the public through the National Technical Information Service www.ntis.gov.	
19 Security Classification (of this report) Unclassified	**20 Security Classification (of this page)** Unclassified	**21 No. of pages** 91	**22 Price**

Form DOT F 1700.7 (8-72)

This page intentionally left blank.

Large Box Study on Granular Base Options for Portland Cement Concrete Pavements

Final Report

Prepared by

Tanya N. Walkenbach, Ph.D.
Jie Han, Ph.D., P.E., F.ASCE
Robert L. Parsons, Ph.D., P.E.
Zexia Li

The University of Kansas

A Report on Research Sponsored by

THE KANSAS DEPARTMENT OF TRANSPORTATION
TOPEKA, KANSAS

and

THE UNIVERSITY OF KANSAS
LAWRENCE, KANSAS

March 2021

PREFACE

The Kansas Department of Transportation's (KDOT) Kansas Transportation Research and New-Developments (K-TRAN) Research Program funded this research project. It is an ongoing, cooperative and comprehensive research program addressing transportation needs of the state of Kansas utilizing academic and research resources from KDOT, Kansas State University and the University of Kansas. Transportation professionals in KDOT and the universities jointly develop the projects included in the research program.

NOTICE

The authors and the state of Kansas do not endorse products or manufacturers. Trade and manufacturers names appear herein solely because they are considered essential to the object of this report.

This information is available in alternative accessible formats. To obtain an alternative format, contact the Office of Public Affairs, Kansas Department of Transportation, 700 SW Harrison, 2nd Floor – West Wing, Topeka, Kansas 66603-3745 or phone (785) 296-3585 (Voice) (TDD).

DISCLAIMER

The contents of this report reflect the views of the authors who are responsible for the facts and accuracy of the data presented herein. The contents do not necessarily reflect the views or the policies of the state of Kansas. This report does not constitute a standard, specification or regulation.

Abstract

With the depletion of natural resources and limited funding for necessary pavement construction and rehabilitation, recycled concrete aggregate (RCA) and reclaimed asphalt pavement (RAP) are potential alternatives to the virgin granular base (VGB) typically used. The addition of geosynthetics at the interface of base course and subgrade can stabilize base course sections through separation, lateral restraint, and a tensioned membrane effect.

This large-scale box study focused on two different granular base options (VGB and RCA) with geosynthetic stabilization for concrete pavement applications. Unpaved road tests under cyclic loading were first conducted on these granular bases over weak subgrade to evaluate the benefits of three types of geosynthetics (nonwoven geotextile, woven geotextile, and triaxial geogrid) and replacement of VGB with RCA in the improved performance (permanent deformation and stress reduction) and properties (resilient modulus and modulus of subgrade reaction). The nonwoven geotextile was selected for three concrete paved roads with VGB and RCA over the same subgrade under cyclic loading. Displacement transducers and earth pressure cells were placed in the test sections to monitor resilient and permanent deformations on the section surface and vertical interface stresses between base course and subgrade.

For the unpaved test sections, the measured resilient and permanent deformations and the interface stress reduction were analyzed to evaluate the benefits of geosynthetics and replacement of VGB with RCA. The modified Burmister solution and the stress reduction method were used to back-calculate the resilient moduli (M_r) of the granular bases for all the test sections. Back-calculated resilient moduli were correlated with the accumulated permanent deformations to assess these methods. The American Association of State Highway and Transportation Officials (AASHTO, 1993) design chart was used to estimate the composite subgrade reaction moduli of the unpaved test sections based on the back-calculated resilient moduli (M_r) of the granular bases.

The three concrete paved sections and the benefits of the nonwoven geotextile and the replacement of VGB with RCA were evaluated in terms of their total and permanent displacements and base course-subgrade interface stresses. Based on the measured vertical displacements at the loaded corner, Westergaard's (1926) method was used to back-calculate the subgrade reaction

moduli of these sections and estimate the tensile stresses in the concrete slabs. The back-calculated subgrade reaction moduli of these concrete paved sections were compared with those calculated based on the unpaved road sections.

The key findings of this study are: (1) geosynthetics were effective in reducing the permanent deformations of both VGB and RCA base courses over the weak subgrade in unpaved and concrete paved roads under cyclic loading; (2) RCA was stronger and stiffer than VGB and replacement of VGB with RCA reduced the permanent deformations in unpaved and concrete paved roads under cyclic loading; (3) the resilient modulus of the base course in an unpaved road section back-calculated by the modified Burmister solution with the mechanistic-empirical damage model was correlated well with the accumulated permanent deformation of the unpaved road section; (4) the modulus of subgrade reaction of a base over a subgrade estimated by the AASHTO design chart with the back-calculated resilient modulus of the base from an unpaved road test was similar to that back-calculated by the Westergaard solution based on the displacement at the loaded corner; (5) the accumulated permanent deformation of an unpaved or concrete paved section increased with the reduction of the subgrade reaction modulus in a semi-logarithmic relationship; and (6) geosynthetic stabilization and/or replacement of VGB with RCA increased the resilient modulus and the subgrade reaction modulus of a test section.

Acknowledgements

This research project was financially sponsored by the Kansas Department of Transportation (KDOT). Mr. Luke Metheny, Chief Geotechnical Engineer (KDOT Bureau of Structures and Geotechnical Services), Mr. James Brennan, formerly Chief Geotechnical Engineer, and Mr. Nat Velasquez, Pavement Design Engineer (KDOT Bureau of Road Design) are the project monitors. Ms. Amanda Keeney, Engineering Associate I (KDOT Bureau of Structures and Geotechnical Services) performed careful review of this report and provided many useful comments and suggestions. Ms. Audrey Atkinson, NHI & Research Coordinator (KDOT Bureau of Research) provided administrative coordination. The laboratory manager, Mr. David Woody and technician, Mr. Kent Dye, in the Department of Civil, Environmental, and Architectural Engineering (CEAE) at the University of Kansas (KU) provided their technical support. Furthermore, this experimental study received assistance from several former and current graduate and undergraduate students at KU CEAE: Dr. Jun Guo, Dr. Madan Neupane, Dr. Saif Jawad, Dr. Mahdi Al-Naddaf, Dr. S. Mustapha Rahmaninezhad, Hao Liu, Cassidy Diebold, Daniel Rich, Jesus Leos, Zeyad Dessouki, Ashley Underwood, Audrey Carroll, Brandon Tabor, and Luke Spriggs. All the above support and help are greatly appreciated.

Table of Contents

List of Tables

List of Figures

Chapter 1: Introduction and Background

1.1 Project Description

For Portland Cement Concrete Pavements (PCCP) in small communities or areas, granular bases have been placed on natural subgrade as pavement foundations instead of cement-treated bases and lime-treated subgrade. In recent years, recycled concrete pavement (RCP) aggregate and reclaimed asphalt pavement (RAP) aggregate have been increasingly used as a base course material for roadway construction. To minimize intermixing between aggregate and subgrade soil as well as reduce lateral spreading of granular base under traffic loading, geosynthetics, such as nonwoven geotextile, woven geotextile, and geogrid, have been used. Despite their potential benefits, recycled aggregate and geosynthetics have not been commonly used together in base course for concrete pavements. Therefore, the performance of granular bases (including recycled aggregate) with geosynthetics and the benefits of geosynthetics to the improved performance of concrete pavements have not been well evaluated. A comprehensive study is warranted but requires significant funding and time.

This study focused on investigating the relative benefits of granular base options with geosynthetics for concrete pavements. To achieve this objective, this study was conducted in two phases: (1) evaluation of unpaved roads (i.e., granular bases over subgrade) as pavement foundations with three different types of aggregate materials (virgin aggregate, recycled concrete aggregate, and reclaimed asphalt pavement aggregate) and three different types of geosynthetics (nonwoven geotextile, woven geotextile, or triaxial geogrid), and (2) evaluation of concrete pavements on two types of aggregate materials with one type of a selected geosynthetic. Cyclic plate loading tests were conducted in a large box on different granular bases, either non-stabilized or stabilized by geosynthetics, without and with concrete pavements, to evaluate their performances under traffic loading. Their performances were first evaluated without any concrete pavement. Two granular base options with one type of geosynthetic were selected based on performance and economy, and these road sections were then constructed and tested with concrete pavements.

1.2 Review of Concrete Pavement Design

Several methods (empirical, statistically-based, and mechanistic-empirical) are available for the design of unpaved roads, and asphalt and concrete pavements. Since the focus of this study was on the geotechnical aspects of concrete pavements, i.e., the reactions of the pavement foundations (base course, geosynthetic, and subgrade) under concrete pavements, the design method for concrete pavements will be reviewed. Considering the plate loading tests first conducted on unpaved roads as pavement foundations to evaluate the granular base options with geosynthetics, the design methods for unpaved roads and flexible pavements will be reviewed as well.

Westergaard (1926) developed early theoretical solutions for computing stresses and deflections of concrete pavements. In the development of these solutions, he treated a pavement foundation (i.e., subbase over subgrade or subgrade) as a series of springs and introduced the modulus of subgrade reaction, *k*, as a constant stiffness value for these "springs" across a homogeneous subgrade. Westergaard stated that variations of *k* up to four orders of magnitude (from 50 psi/in. to 200 psi/in.) yield only minor changes in the estimated stresses in a concrete slab, so the assumption of a uniform modulus of subgrade reaction across the slab is valid. Westergaard defined a radius of relative stiffness, *l*, of the concrete slab based on the slab thickness and modulus, and the modulus of subgrade reaction as follows in Equation 1.1; this radius of relative stiffness corresponds to radius of gyration of the slab.

$$l = \sqrt[4]{\frac{Eh^3}{12(1-\mu^2)k}} \qquad \textbf{Equation 1.1}$$

Where:

E = elastic modulus of the concrete slab,

h = thickness of the concrete slab,

μ = Poisson's ratio of concrete, and

k = modulus of subgrade reaction.

Figure 1.1 depicts three loading cases Westergaard considered in his 1926 theory. Critical tension in the slab was identified as top-of-slab tension for corner loading, bottom-of-slab tension for center loading, and bottom-of-slab tension under edge loading. His theory for the loading axes and slab behavior changes with the load locations (Westergaard, 1926). In the current study, only

corner loading on concrete slabs was simulated in the large box tests; therefore, the theory for this loading condition is reviewed below.

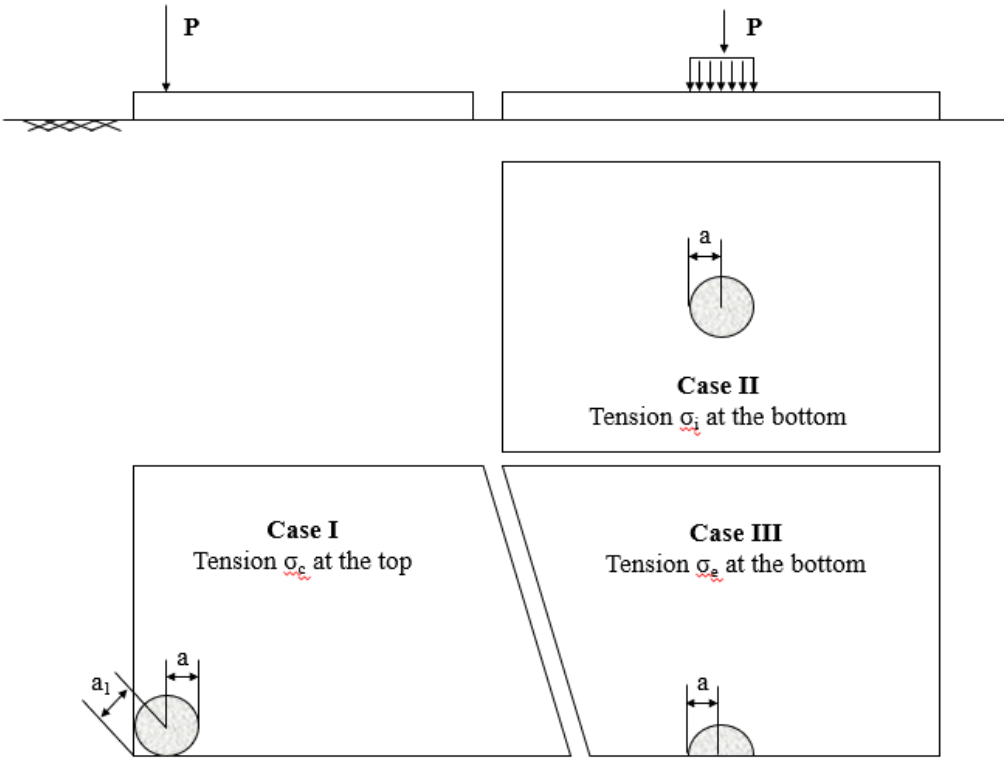

Figure 1.1: Loading Cases Analyzed by Westergaard (1926)

Deflection and maximum stress in the concrete slab due to corner loading can be calculated using Equation 1.2 and Equation 1.3, respectively, as obtained by Westergaard (1926).

$$z_c = \frac{P}{kl^2}\left(1.1 - 0.88\frac{a_1}{l}\right) \qquad \textbf{Equation 1.2}$$

Where:

z_c = the deflection of the slab at the corner due to corner loading,

P = the applied force,

k = the modulus of subgrade reaction,

l = the radius of relative stiffness, and

a_1 = the distance from the corner to the center of the loaded area,

$a_1 = a\sqrt{(2)}$, where a = the radius of the circular loaded area.

$$\sigma_c = \frac{3P}{h^2}\left[1 - \left(\frac{a_1}{l}\right)^{0.6}\right]$$ **Equation 1.3**

Where:

σ_c = the maximum tensile stress in the slab due to corner loading, and

h = the thickness of the slab.

These formulae consider the changes in bending moment per unit width and the secant modulus of the slab. The location of the maximum moment due to corner loading, x_1, is found based on incremental moments using Equation 1.4.

$$x_1 = 2\sqrt{a_1 l}$$ **Equation 1.4**

Where:

x_1 = the maximum moment location due to corner loading,

a_1 = the distance from loaded corner to center of the circular load plate, and

l = the radius of relative stiffness.

Westergaard (1926) found that greater changes in the deflection and stress occurred from the slab corner to the center of the load plate as shown in Figure 1.1. Changes in the k-value yielded only small changes in the slab stress under corner loading.

1.3 Layered Elastic Theory

Burmister (1945) published a series of three papers that address the continuity and reactions of layered soil systems. His theory was originally developed for the design of airport pavements and foundations. His two-layer theory has been widely used in the design of unpaved roads and flexible pavements.

Burmister (1945) made the assumptions in his two-layer system that conform to the theory of elasticity (see Figure 1.2). Both layers in the system are assumed to have infinite horizontal extents. The upper layer is finite with a thickness *h* but is underlain by a lower layer that is infinitely deep. The upper layer beyond the loading area has no normal or shear stress (i.e., the boundary condition) and the lower layer has zero displacement at infinite depth. Burmister also assumed two continuity conditions between two layers: (1) they are in continuous contact and move together elastically at all contact locations (i.e., all displacements and stresses at the interface are equal), and (2) they have a frictionless interface (i.e., only normal stress and displacement are continuous). His solutions satisfy the force equilibrium in the theory of elasticity. Furthermore, Burmister

(1945) developed solutions for a three-layer flexible pavement system with similar assumptions, boundary conditions, continuity conditions, and force equilibrium as in the two-layer system; however, most of the discussion in the literature and also herein focused on the application to a two-layer system.

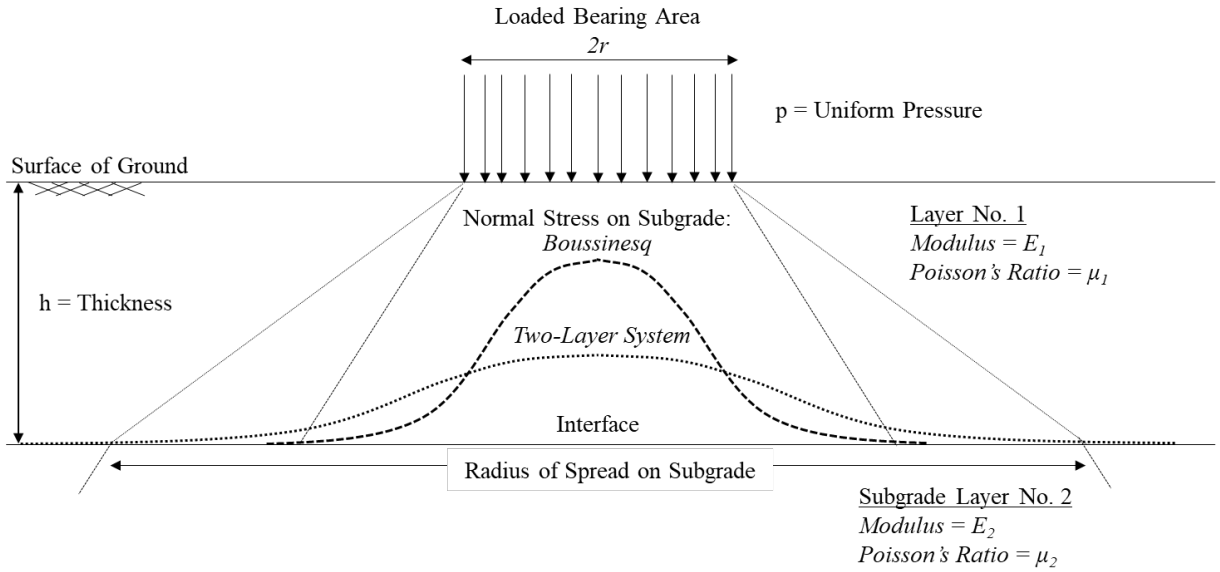

Figure 1.2: Burmister's schematic for the two-layer soil system
Source: Burmister (1945)

Figure 1.2 illustrates the difference in the vertical (or normal) stress distributions in a homogenous medium (by the Boussinesq solution) and a two-layer system (by the Burmister solution). When the upper layer has a higher modulus than the lower layer, the maximum vertical stress in the two-layer system is lower than that in the homogenous medium. Burmister (1945) illustrated the concept of load distribution by a distribution angle in Figure 1.2.

Burmister (1945) confirmed the validity of the Boussinesq solution for a surface deformation under a circular, flexible load, with the assumption of Poisson's ratio (μ) of both soil layers equal to 0.5, using a settlement coefficient F as shown in Equation 1.5.

$$\mathbf{w} = \begin{cases} \frac{\mathbf{1.5pr}}{\mathbf{E_2}} \mathbf{F}_w \left[\frac{\mathbf{r}}{\mathbf{h}}, \frac{\mathbf{E_2}}{\mathbf{E_1}}\right] & \textbf{(flexible plate)} \\ \frac{\mathbf{1.18pr}}{\mathbf{E_2}} \mathbf{F}_w \left[\frac{\mathbf{r}}{\mathbf{h}}, \frac{\mathbf{E_2}}{\mathbf{E_1}}\right] & \textbf{(rigid plate)} \end{cases}$$ **Equation 1.5**

Where:

w = the surface deflection of a two-layer system,

p = the applied pressure,

r = the radius from the center of the circular load area,

h = the thickness of the upper soil layer,

E_1 and E_2 = the elastic moduli of the upper and lower soil layers, and

F_w = the settlement coefficient (a function of E_1/E_2 and h/r)

Figure 1.3 depicts Burmister's chart to determine the coefficient F_w based on the full continuity interface assumption. For a rigid plate, a factor of 1.18 should be used instead of 1.5 based on the elastic solution.

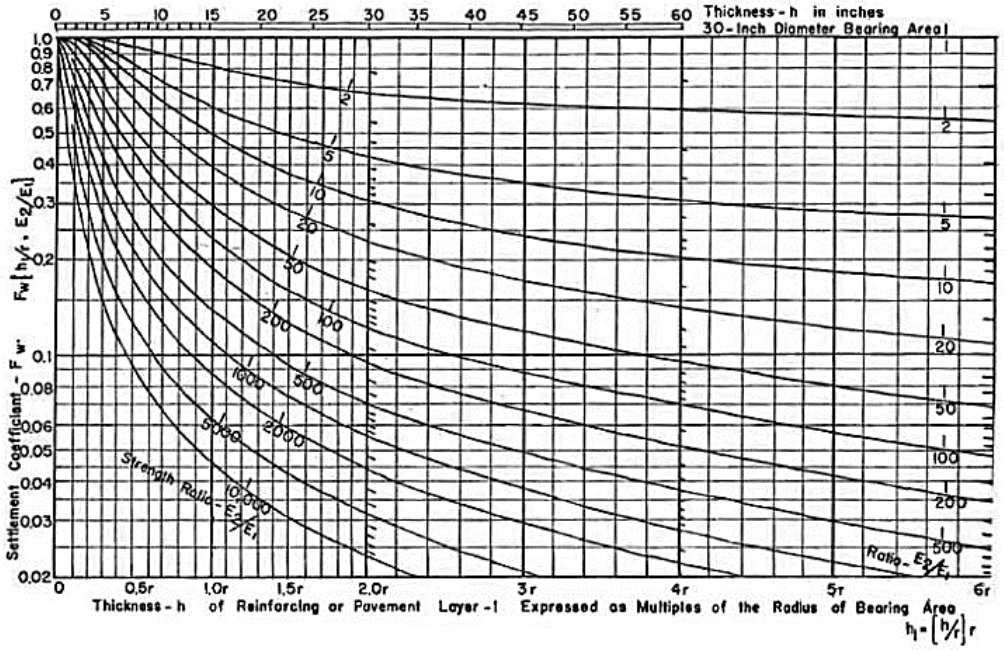

Figure 1.3: Settlement coefficient F_w chart

Source: Burmister (1945)

Figure 1.4a illustrates the concept of the stress distribution angle as discussed earlier. Based on this concept, the stress distribution angle can be calculated from the maximum vertical stress at

the center between the base course and the subgrade induced by an applied pressure as displayed in Equation 1.6.

$$\tan \alpha_1 = \frac{1}{h}\left[\sqrt{\frac{r^2 p}{\Delta \sigma_{zi}}} - r\right] \qquad \textbf{Equation 1.6}$$

Where:

α_1 = the stress distribution angle,

h = the thickness of the base course,

r = the radius of the applied pressure at the base course surface,

p = the applied pressure at the base course surface, and

$\Delta\sigma_{zi}$ = the maximum additional vertical stress at the base course / subgrade interface.

Figure 1.4b shows the reduced vertical stresses at different layers as a function of the elastic modulus ratio between two adjacent layers in the three-layer pavement system. The vertical stresses can be used to calculate the vertical strains of all the layers when their moduli and Poisson's ratios are known. Burmister (1945) concluded that a high-modulus upper (base course) layer overlying a low-modulus lower (subgrade) layer increased the stress distribution angle and thus reduced the vertical stress at depth directly beneath the center of the applied load.

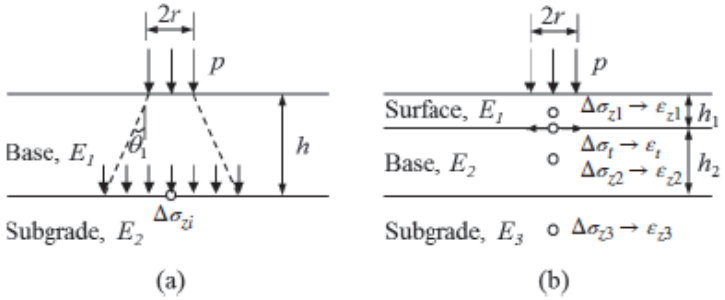

Figure 1.4: Stress distribution in: (a) unpaved roads and (b) paved roads

Source: Han (2015)

Burmister (1958) introduced several design charts that relate the reduced vertical stress at depth to the ratio of the elastic modulus of base course to subgrade, assuming the overlying layer has an equal or higher elastic modulus. Figure 1.5 displays the relationship between the vertical stress coefficient and the normalized depth at different modulus ratio of upper to lower layer (E_1/E_2). The vertical stress coefficient is defined as the reduced vertical stress at depth (σ_z) divided

by the applied pressure at the surface (p). The normalized depth is a given depth (z) divided by the load radius (r). It is shown that the vertical stress reduction coefficient decreases with the increase of the modulus ratio, indicating that the higher modulus layer overlying the lower modulus layer results in greater stress reduction and a wider stress distribution radius at depth.

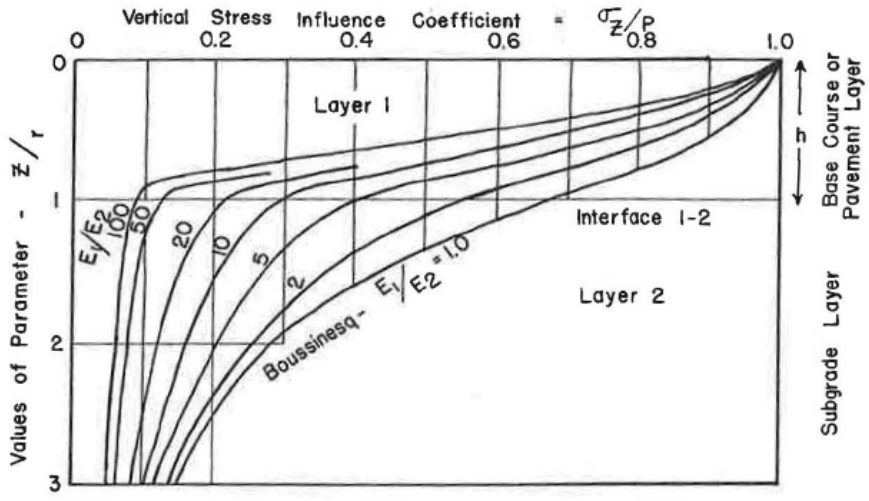

Assuming r/h=1.0 and μ=0.50

Figure 1.5: Vertical stress reduction chart
Source: Burmister (1958)

Figure 1.6 is similar to Figure 1.5 except that the vertical stress is only observed at the interface between the base course and the subgrade layer, so various radii in relation to the base course thickness may be evaluated. As the radius of the applied load at the surface increases at the same stress reduction coefficient, the modulus ratio increases. On the other hand, at a constant radius-to-thickness ratio, an increase in the stress reduction ratio (i.e., higher vertical stress) at the interface results in a decrease in the modulus ratio. Both charts assume Poisson's ratio of 0.50. These charts as well as Equation 1.6 can be used to estimate the elastic moduli of the pavement layers when the vertical stresses at the interface between the base course and the subgrade are measured.

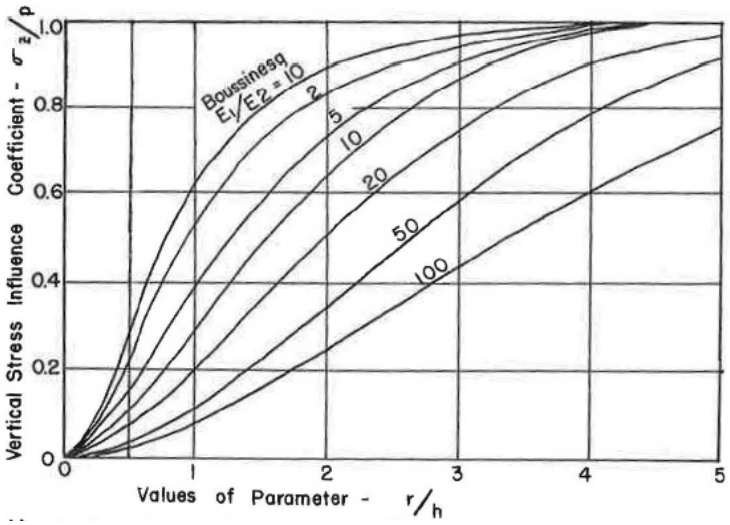

Assuming Poisson's ratio μ= 0.50

Figure 1.6: Vertical stress reduction at the interface between base course and subgrade
Source: Burmister (1958)

Sun, Han, and Corey (2017a) modified Burmister's layered elastic solution by including a geosynthetic at the interface to determine the elastic responses of a geosynthetic-stabilized base course over a weak subgrade. Sun et al. (2017a) and Sun, Han, Crippen, and Corey (2017b) also adopted the permanent deformation empirical formula in the AASHTO (2015) Mechanistic-Empirical Design Guide (MEPDG) to predict the permanent deformation of the geosynthetic-stabilized unpaved road. This empirical formula, to be discussed later, requires the input of resilient modulus of the subgrade and the modulus ratio E_1/E_2. The Sun et al. (2017a, 2017b) solution was developed by modifying the Burmister solution and adopting the MEPDG permanent deformation empirical formula and has been incorporated in a MATLAB code. When the measured permanent deformation of a road surface and the resilient modulus of the subgrade are known, the equivalent resilient modulus of the geosynthetic-stabilized base course section as one composite layer can be back-calculated (Sun et al., 2017a). The Sun et al. (2017a, 2017b) solution was used in this study to analyze the results from unpaved road tests under plate loading.

1.4 1993 AASHTO Pavement Design Guide

The American Association of State Highway and Transportation Officials (AASHTO) published its original pavement design guide in 1986, then updated and published the widely used

design guide in 1993 (often referred to as the 1993 AASHTO Pavement Design Guide). This design guide identified the number of 80-kN (18-kip) equivalent single axle loads (ESALs) that a given pavement section can undergo, based on engineering design values for a given pavement section, a confidence level in the model, and an allowable change in serviceability over a given pavement lifespan. This guide considers several key design factors, including erosion loss of support (Figure 1.7), resilient modulus of roadbed soil, traffic in terms of ESALs, pavement management, rehabilitation, reliability, serviceability, and the vision for mechanistic-empirical design procedures (AASHTO, 1986, 1993). Figure 1.7 provides an approach of correcting the modulus of subgrade reaction by considering the loss of support in concrete pavements due to erosion and loss of concrete-soil contact.

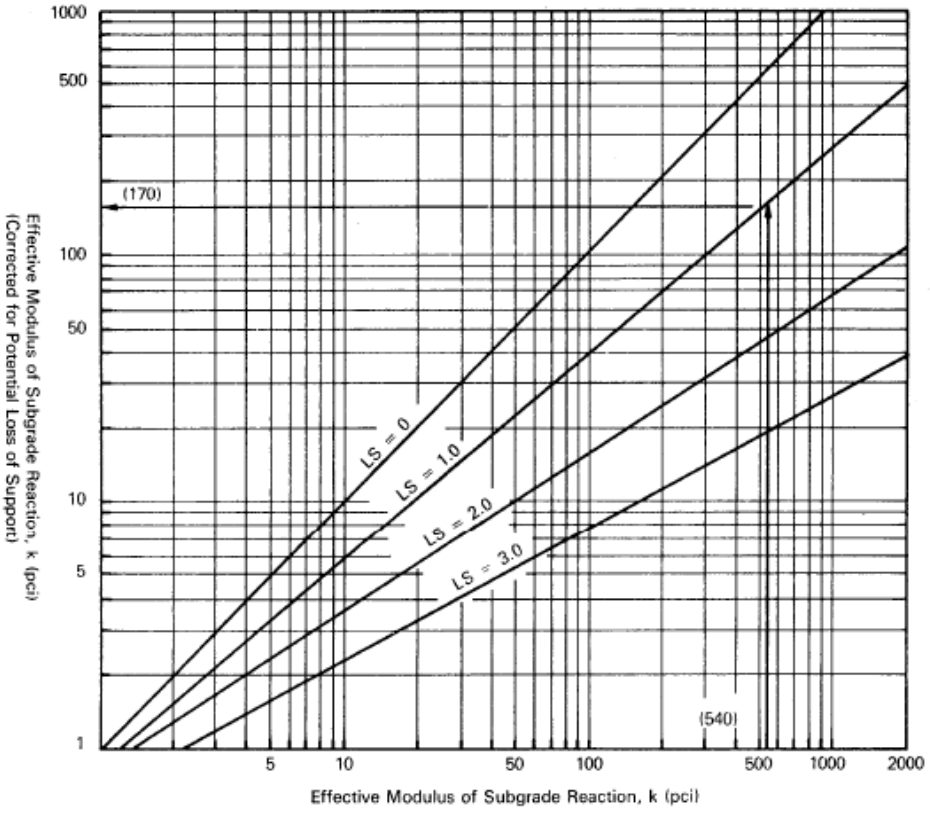

Figure 1.7: Loss of support correction for modulus of subgrade reaction
Source: AASHTO (1993)

For concrete pavement design, the number of ESALs a pavement section can endure can be estimated by Equation 1.7. This long equation focuses heavily on the properties of the concrete

slab but also includes the modulus of subgrade reaction underneath the concrete slab (i.e., the k-value). The emphasis on loss of support (Figure 1.7) due to erosion beneath the slab is of great importance for the design input k-value in Equation 1.7 (AASHTO, 1993) indicating that a stabilizing geosynthetic layer could be imperative to sustainable concrete pavements.

$$\log_{10} W_{18} = Z_R S_0 + 7.35 \log_{10}(D+1) - 0.06 + \frac{\log_{10}\left(\frac{\Delta PSI}{4.5-1.5}\right)}{1+\frac{1.624\times 10^7}{(D+1)^{8.46}}} + (4.22 - 0.32 p_t)\log_{10}\left\{\frac{S_c C_d (D^{0.75}-1.132)}{215.63 J\left[D^{0.75} - 18.42 \Big/ \left(E_c/k\right)^{0.25}\right]}\right\}$$

Equation 1.7

Where:

W_{18} = the number of Equivalent Single Axle Loads (ESALs),

D = the slab thickness,

E_c = the concrete slab elastic modulus,

S_c = the slab modulus of rupture,

Δpsi = the change in serviceability,

p_t = the terminal serviceability,

C_d = the drainage coefficient,

S_0 = the overall standard deviation,

Z_R = the normal standard deviate (based on reliability), and

k = the modulus of subgrade reaction.

The modulus of subgrade used in this formula is a composite value for the system where a base or subbase exists above the subgrade (see Figure 1.8). The AASHTO guide explicitly stated that direct measure of composite modulus of subgrade reaction using standard static plate load testing will not produce accurate results. To estimate the composite modulus of subgrade reaction using the design chart in Figure 1.8, the resilient modulus of the subgrade is needed, which can be estimated in the laboratory or in the field. In the laboratory, the AASHTO T 307 (2017) procedure using a triaxial shear device with a dynamic load system can be used to determine the resilient

modulus of an aggregate sample. The AASHTO guide relates the resilient modulus to the modulus of subgrade reaction, assuming a 762-mm (30-inch)-diameter plate and 69-kPa (10-psi) applied load. This guide suggested that the modulus of subgrade reaction for fine-grained subgrade is equal to the resilient modulus of the subgrade divided by 19.4, i.e., k is equal to M_r (psi)/19.4. The 1993 AASHTO guide correlates California Bearing Ratio (CBR) to the resilient modulus using Equation 1.8 for fine-grained soils with CBR less than 10 and using Equation 1.9 for an aggregate base material. Loss of support should also be applied to the k-value using Figure 1.7. The recommended loss of support is 1.0 to 3.0 for unbound granular materials, 2.0 to 3.0 for natural subgrade, and 0.0 to 1.0 for cement- and bituminous-treated base courses. This design guide (AASHTO, 1993) does not account for the benefit of geosynthetic stabilization.

$$\boldsymbol{M_r(psi) = 1500 \times CBR \rightarrow M_r(MPa) = 10.3 \times CBR} \qquad \textbf{Equation 1.8}$$

$$\boldsymbol{E_b(MPa) = 17.6CBR^{0.64}} \qquad \textbf{Equation 1.9}$$

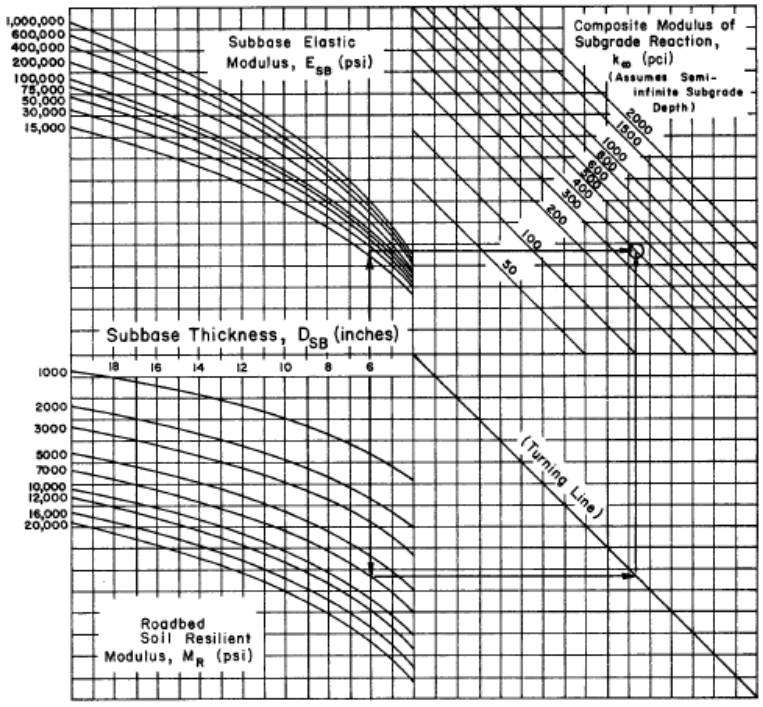

Figure 1.8: Composite modulus of subgrade reaction
Source: AASHTO (1993)

1.5 Mechanistic-Empirical Pavement Design Guide

Mechanistic-Empirical Pavement Design Guide (MEPDG) is a recently developed pavement design guide to replace the 1993 AASHTO pavement design guide. The MEPDG consists of mechanistic and empirical components. The mechanistic components are primarily based on the layered elastic theory by Burmister (1945, 1958) for asphalt pavements and the Westergaard solutions (Westergaard, 1926) for concrete pavements. The empirical component uses the calculated elastic responses from the mechanistic component as inputs in empirical damage models to predict distresses of pavements. The MEPDG requires design inputs and material parameters necessary for use in the AASHTOWare software. The software uses neural network structural response models based on ISLAB2000 finite element analysis runs for concrete pavements. This analysis uses the radius of relative stiffness as identified in Equation 1.10 that depends on the modulus of subgrade reaction (NCHRP, 2004).

$$l = \sqrt[4]{\frac{E_{PCC} h_e^3}{12(1-\mu_{PCC}^2)k}} \qquad \textbf{Equation 1.10}$$

Where:

l = the radius of relative stiffness (typically 0.56 to 2.00 m),

E_{PCC} = the elastic modulus of Portland cement concrete,

h_e = the concrete slab thickness,

μ_{PCC} = Poisson's ratio of concrete, and

k = the modulus of subgrade reaction.

The MEPDG divides concrete pavements into jointed plain concrete pavements (JPCP) and continuously reinforced concrete pavements (CRCP). Critical design criteria for JPCP are transverse cracking of 10% to 45%, transverse joint faulting of 2.5 to 5 mm (0.1 to 0.2 in), and International Roughness Index (IRI) pavement smoothness of 2.3 to 3.9 m per km (146 to 247 in./mi). CRCP performance criteria include load transfer efficiency (LTE) greater than 95% and crack width of 0.5 mm (0.02 in.), IRI smoothness, and punchouts of 6 to 12 per km (10 to 19 per mi). Design input parameters include climate, traffic, drainage, pavement structure and thermal expansion properties. Distance of the wheel path from the edge of the concrete slab and the deviation of that path increase cracking potential in both JPCP and CRCP. Infiltration and drainage

potential of the pavement is used to estimate water entering the base course layer from precipitation at four levels: none, minor (10%), moderate (50%), or extreme (100%) (NCHRP, 2004).

For pavement structures, the AASHTOWare software converts the resilient moduli of multiple layers underlying the pavement and base course to a dynamic k-value. This value differs from the Westergaard static k-value as it is estimated from multiple deflections from a 40-kN (9-kips), 150-mm (6-in.) falling weight deflectometer (FWD) model atop a concrete pavement. Despite the distinction between static and dynamic moduli, the theory for the underlying layer acting like a series of springs beneath the concrete pavement matches the Westergaard method. The AASHTOWare software similarly converts the pavement and base course into an equivalent rigid layer atop the equivalent subgrade for neural network modeling as shown in Equation 1.11 (NCHRP, 2004). This equation implies that a reaction will occur between the base course and the subgrade, and that the base course will not be the mode of failure due to loading at the pavement surface. This analysis accounts for both temperature and tire loading.

$$h_{eff} = \sqrt[3]{h_{PCC}^3 + \frac{E_{base}}{E_{PCC}} h_{base}^3 + 12\left[h_{PCC}\left(x - \frac{h_{PCC}}{2}\right)^2 + \frac{E_{base}}{E_{PCC}}\left(h_{PCC} + \frac{h_{base}}{2} - x\right)^2 h_{base}\right]}$$

Equation 1.11

Where:

h_{eff} = the effective pavement thickness,

h_{PCC} = the concrete thickness,

h_{base} = the base course thickness,

E_{base} = the base course elastic modulus,

E_{PCC} = the concrete elastic modulus, and

x = the distance between the neutral plane and the top surface of the PCC layer.

Behavior of pavement sections is dependent upon the applied stress, strength properties, and incremental damage incurred by repeated load cycles (i.e., traffic). Tseng (1988) acknowledged that the resilient modulus of a pavement foundation layer was stress-dependent as shown in Equation 1.12.

$$M_r = a\sigma_\theta{}^b\sigma_d{}^c$$ **Equation 1.12**

Where:

M_r = the resilient modulus of subbase/subgrade layer,

σ_θ = the bulk stress,

σ_d = the deviator stress, and

a, b, and c = regression constants.

Tseng and Lytton (1989) identified that permanent deformations for pavement foundation layers including unbound granular materials are dependent upon the number of cycles and the unique relationship between their permanent and resilient deformations. NCHRP (2004) modified the original Tseng and Lytton (1989) model as the damage model for unbound granular layers included in the MEPDG as shown in Equation 1.13 and Equation 1.14.

$$\delta_{p,3} = k_b\delta_{r,1}\left(\frac{\varepsilon_0}{\varepsilon_r}\right)_b e^{-\left(\rho_b/N\right)^{\beta_b}}$$ **Equation 1.13**

Where:

$\delta_{p,3}$ = the permanent deformation at the surface of a base course,

k_b = the calibration factor,

$\delta_{r,1}$ = the resilient deformation at the surface of the base course,

N = the number of load cycles, and:

$$\begin{cases} \beta = 10^{\left(-0.61119-0.017638W_{c(b,s)}\right)} \\ \rho_{(b,s)} = 10^9\left[\frac{-4.89285}{1-\left(10^9\right)^{\beta_b}}\right]^{1/\beta_b} \\ \left(\frac{\varepsilon_0}{\varepsilon_r}\right)_{(b,s)} = \frac{0.15\cdot e^{\rho_b{}^{\beta_b}}+20\cdot e^{\left(\rho_b/10^9\right)^{\beta_b}}}{2} = \left(\frac{\varepsilon_p}{\varepsilon_r}\right)_{N\to\infty} \end{cases}$$ **Equation 1.14**

Where:

$W_{c\ (b,s)}$ = the moisture content of the base course (b) or subgrade (s),

ε_p = the accumulated permanent vertical strain, and

ε_r = the (average) vertical resilient strain.

The MEPDG designates that the evaluation of damage beneath the concrete slab should be performed separately from the damage of the concrete slab. Equation 1.13 is the rutting formula for flexible pavements, which may be used for unpaved roads. This model is recommended by

NCHRP for modeling the damage in the base course and subgrade layers beneath concrete pavements (NCHRP, 2004).

1.6 Recycled Aggregate Base

Aggregates for road construction are in sustainable demand. Since 1995, the per capita usage of aggregates in the United States has not fallen below 7 tons (Ober, 2017). In 2016, the U.S. produced 2.8 million tons of construction aggregates, and production occurred in all 50 states (Ober, 2017). Construction aggregates comprised 34% of U.S. production by revenue and 87% of mineral production tonnage in 2016 (Ober, 2017). It is estimated that a person born in 2017 in the U.S. will consume over 1.4 million pounds of stone, sand, and gravel, or materials used in construction (Ober, 2017). These steady trends in demand necessitate the identification of low-cost sources to meet continuing construction demands. With an established roadway system in the U.S., focus of road construction should include cost-saving and environmentally friendly measures for both rehabilitation of existing roads and construction of new roads.

Recycled (or reclaimed) concrete aggregate (RCA) (also known as reclaimed concrete material, RCM, or recycled concrete pavement, RCP) has been used as a base course material throughout the United States. AASHTO has designated RCA as an aggregate base course material (AASHTO, 2015). RCA has also been suggested to be used in cement-stabilized subbases based on cost and environment by federal and state agencies (Jung, Zollinger, Cho, Won, & Wimsatt, 2012). Han and Thakur (2015) noted that the mechanical properties (mainly strength and stiffness) and long-term durability (breakage and abrasion) of recycled aggregates may not be sufficient for load support. To improve its properties, RCA has been blended with virgin aggregates or stabilized by chemical additives. However, the blending of RCA with virgin aggregate still consumes natural resources and the chemical stabilization is not environmentally friendly. Possible use of geosynthetics with RCA may improve the material properties of the RCA as well as ensure sustainability of its uses but requires comprehensive research.

Reclaimed asphalt pavement (RAP) is milled out of existing pavements, crushed, and screened into coarse and fine fractions as deemed necessary by the asphalt mix design and typically processed for recycle into new asphalt mixes. Recycling RAP into new asphalt mixes saves in raw

aggregate needs but more importantly in the reduction in need for expensive asphalt oil. The finer fraction of processed RAP will have a greater oil recovery, but it also increases the amount of waste fines that must be rejected from the mix. Since aged asphalt in RAP may change the behavior of the new asphalt mixes, the amount of RAP used in the mixes is often limited. Researchers have explored the possibility of using RAP as base course materials in roadway construction. Because RAP is crushed and screened, it can be produced to meet base course specifications for gradation and plasticity index. Thakur and Han (2015) provided a literature review on the recent development of RAP bases treated for highway construction including the use of RAP aggregates with geosynthetics (mostly geocell). Therefore, such a review will not be repeated herein.

1.7 Geosynthetic Stabilization of Roads

Geosynthetics have widely been used for the stabilization of unpaved roads and asphalt pavements. Han and Thakur (2015) provided a summary of the state-of-practice for geosynthetic-stabilized recycled aggregates including recycled concrete aggregate (RCA), reclaimed asphalt pavement (RAP), and recycled (railroad) ballast (RB). Geosynthetics provide three major benefits when used to stabilize base and subbase: separation, lateral restraint, and tensioned membrane effect (Maxwell, Kim, Edil, & Benson, 2005). Separation and preservation of base course layers are vital to the longevity of concrete pavements. Geogrid and geotextile can provide lateral restraint to aggregates through interlocking with geogrid apertures or friction with geotextile surfaces to minimize lateral movement of aggregates under cyclic loading. Since the vertical component of a tensile force in the tensioned membrane resists a wheel load, large rutting of a road (typically more than 75 mm or 3 in.) is necessary for the tensioned membrane to mobilize a large tensile force and be effective. However, concrete pavements do not allow large vertical deformation and start to crack at a vertical deformation of less than 13 to 25 mm or 0.5 to 1.0 in., which is not large enough to mobilize the tensioned membrane effect. Therefore, limited studies and uses of geosynthetics in concrete pavements are found in the literature. However, several methods are available in the literature to design geosynthetic-stabilized unpaved roads and asphalt pavements. Two relevant design methods are reviewed below.

1.7.1 Design of Geosynthetic-Stabilized Roads

Giroud and Han (2004a, 2004b) did extensive work to develop a generic design method for unpaved roads when base course is stabilized with geosynthetics, particularly addressing the use of geogrid. This method takes into account the use of geosynthetics by considering the reduction in distribution angle with repeat cyclic loads, the resilient moduli of the base course and subgrade, the strength of the subgrade, the applied load magnitude and area, the ratio of the load radius to base course thickness, the aperture stability modulus of geosynthetic, and the allowable rut depth. This design method is used to estimate the required base thickness of geosynthetic-stabilized unpaved roads as described in Equation 1.15.

$$h = \frac{a+(b-dJ^2)\left(\frac{r}{h}\right)^{1.5}\log N}{f_E}\left[\sqrt{\frac{P}{\pi r^2 m_c N_c c_u}} - 1\right] r \qquad \textbf{Equation 1.15}$$

Where:

a, b, and d = the constants calibrated by laboratory and field test data;

J = aperture stability (m-N/^{o}) (0 for unreinforced and geotextile-reinforced sections);

r = the radius of equivalent tire contact pressure (m or in.) = √[P/(πp)];

p = the applied tire pressure (kPa or psi);

h = the required base course thickness (m or in.);

N = the number of axle passes;

f_E = the modulus ratio factor;

P = the applied wheel load (kN or lb);

m_c = bearing capacity mobilization coefficient;

N_c = bearing capacity factor (3.14 for unreinforced, 5.14 for geotextile-reinforced, 5.71 for geogrid-reinforced roads); and

c_u = undrained cohesion of subgrade (kPa or psi).

One key concept proposed by Giroud and Han (2004a) is the reduction of the stress distribution angle with the number of applied load cycles until failure (i.e., 75 mm or 3 in. for unpaved roads) as described in Equation 1.16.

$$\tan \alpha_1 = \tan \alpha_0 \left[1 + 0.204 \left(\frac{E_{bc}}{E_{sg}} - 1\right)\right]$$ **Equation 1.16**

Where:

α_1 = the stress distribution angle for a cyclic load,

α_0 = the reference distribution angle for a homogenous medium (the commonly used reference angle in the practice for α_0 is 26.7° [Han, 2015]),

E_{bc} = the modulus of base course, and

E_{sg} = the modulus of subgrade.

This formula was developed based on the vertical stress at the center of the base course-subgrade interface from Burmister's (1958) chart in Figure 1.6.

Sun et al. (2017a, 2017b) modified the Burmister (1945) solution for elastic responses by considering the existence of a geosynthetic layer at the interface of base course and subgrade and adopted the MEPDG damage model to determine the permanent deformation of a geosynthetic-stabilized unpaved road by Equation 1.17, and as illustrated in Figure 1.9.

$$\delta_{p,1} = k_b \cdot p \cdot f_b(E_e, E_s, z, a) \left(\frac{\varepsilon_0}{\varepsilon_r}\right)_b e^{-\left(\rho_b/N\right)^{\beta_b}} + k_s \cdot p \cdot f_s(E_e, E_s, z, a) \left(\frac{\varepsilon_0}{\varepsilon_r}\right)_s e^{-\left(\rho_b/N\right)^{\beta_s}}$$ **Equation 1.17**

Where:

$\delta_{p,1}$ = the permanent deformation at the surface of the base course,

$k_{b,s}$ = the calibration factor,

p= the applied load,

f_b = Burmister's settlement coefficient function,

E_e = the equivalent modulus of the base course with geosynthetic(s),

E_s = the modulus of the subgrade,

N = the number of load cycles, and material properties, $\frac{\varepsilon_0}{\varepsilon_r}$, ρ_b, β_b, and β_s, are listed in Equation 1.14, and

k_s = subgrade calibration factor for MEPDG damage model.

$$k_s = a \cdot e^{-b \cdot CBR_{SG}} \frac{p}{N_c c_u}$$ **Equation 1.18**

Where:

CBR_{SG} = California Bearing Ratio of the subgrade (%),

p = applied pressure,

N_c = 3.14,

c_u = 30*CBR_{SG} (kPa), and

a and *b* are regression constants.

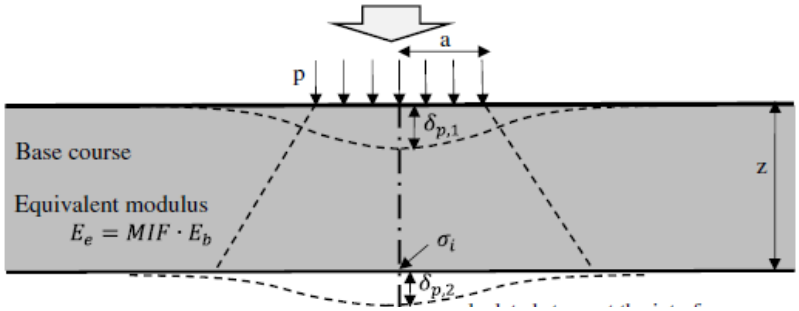

Figure 1.9: Deformations of base course and subgrade under axial plate load
Source: Sun et al. (2017a)

The above design procedure proposed by Sun et al. (2017a) has been included in a MATLAB code. This code requires inputs of load magnitude, number of load cycles, moisture contents, layer CBRs, base course thickness, and subgrade resilient modulus, and the elastic modulus ratio E_1/E_2 and calculates permanent deformation of an unpaved road section. The calibration factor for the base course k_b in the code is treated as a constant value for a given aggregate, but the subgrade calibration factor k_s changes based on the measured interface stress.

1.7.2 Modulus Determination

The moduli of geosynthetic-stabilized base courses can be determined using large-scale plate loading tests based on three methods: (1) resilient deformation, (2) vertical stress at the base-subgrade interface, and (3) permanent deformation.

Large-scale cyclic plate loading tests (CPLTs) have been used to determine resilient moduli of road sections. Qian, Han, Pokharel, and Parsons (2011) used the elastic solution for the deformation of a loading plate on a half-space medium to calculate the subgrade resilient moduli using the measured resilient deformations (i.e., elastic rebounds) from CPLTs and found their values close to the commonly-used correlations in the literature. However, this method was found invalid for geosynthetic-stabilized roads because the inclusion of a geosynthetic may increase the resilient deformations (rebounds) of the roads due to the release of lateral restraint and tensioned membrane during unloading (Sun, Han, Kwon, Parsons, & Wayne, 2015).

As discussed earlier, the measured vertical stress at the center of the base-subgrade interface can be used to back-calculate the stress distribution angle from the base to the subgrade

(Giroud & Han, 2004a). Assuming that the modulus of the subgrade, E_{sg}, does not change, the change in the modulus of the base course, E_{bc}, at different load cycles can be estimated using Equation 1.19.

$$\frac{E_{bc}}{E_{sg}} = 1 + 4.9\left(\frac{\tan\alpha_1}{\tan\alpha_0} - 1\right) \qquad \textbf{Equation 1.19}$$

The stress distribution angle α_1 for each cyclic load can be calculated using the measured vertical stress at the center of the base-subgrade interface and Equation 1.6. Therefore, the relationship between the modulus of the base course and the number of load cycles can be determined if the vertical stress at the center of the base-subgrade interface is measured under each cyclic load. This method is referred to as the stress distribution method later in the report.

Sun et al. (2017a) proposed another method to back-calculate the equivalent resilient modulus of the geosynthetic-stabilized base course using the measured permanent deformation at the surface of the road under cyclic plate loading as shown in Equation 1.17. This method was developed by modifying the Burmister layered elastic solution and using the MEPDG damage model and has been incorporated in the MATLAB code for easy use. This method is referred to as the Burmister (MATLAB) method later in the report. Sun et al. (2017a) found that this method is more reliable to back-calculate the resilient modulus of the geosynthetic-stabilized base than the interface vertical stress method. However, both methods were used in this study to determine the moduli of the geosynthetic-stabilized aggregate bases.

Huang (2004) related the modulus of subgrade reaction (k-value) to the elastic modulus of a soil using Equation 1.20.

$$\boldsymbol{k = \frac{2E_s}{\pi(1-\nu^2)a} = \frac{4pI}{\pi\delta}} \qquad \textbf{Equation 1.20}$$

Where:

p = the applied static pressure;

δ = the deflection of a loading plate;

a = the radius of the plate;

E_s = the elastic modulus of the soil;

ν = Poisson's ratio (assumed to be 0.45 by Huang, 2004); and

I = the settlement influence factor.

The k-value based on the above equation is typically determined using a static plate loading test with a circular plate size of 380 mm in radius (a_s) (Huang, 2004). When a small plate is used, it may yield a high k-value. Under such a condition, the k-value based on the static plate loading test should be corrected by multiplying a dimensional factor of a/a_s. However, this correction is only valid when the soil is uniform.

Chapter 2: Large-Scale Plate Loading Tests

The goal of the test method adopted in this study is to replicate a field condition and evaluate the performance of the base sections to be used in the field. Subgrade conditions at two different strengths were considered. Three different types of aggregate bases including recycled aggregates and three types of geosynthetics were evaluated. One concrete slab thickness was used in this study. Material properties were determined or identified prior to testing, and a plan to control the consistency of the test sections during and after construction was developed. The following sections discuss the concepts, setup, and procedure of the large-scale plate loading tests conducted in this study.

2.1 Material Selection

KDOT engineers were consulted and the approved materials and suppliers list was considered in the selection of materials for this project. Nonwoven geotextile, woven geotextile, and triaxial geogrid were selected based on the KDOT pre-approval list. The virgin granular base (VGB) aggregate source for meeting the KDOT specification for granular bases was located. Recycled concrete aggregate (RCA) and reclaimed asphalt pavement (RAP) aggregate were identified locally in Kansas. The RAP conforming to the KDOT granular base specification was a part of the initial evaluation but not further tested in this study because it exhibited excessive deformations under loading as compared with the other two aggregates (VGB and RCA).

2.1.1 Subgrade

To properly compare the base course options, the variations of subgrade properties should be minimized. To create a consistent subgrade, a blend of processed, powdered kaolin and ASTM C33 sand with water was used. Similar blending procedures for subgrade have been used in prior research (e.g., Guo, Han, Schrock, Sun, & Parsons, 2016).

The ASTM C33 sand came from an aggregate producer in Lawrence, Kansas. This sand was mined from the Kansas River. It is tan to orange in color, clean and free of debris, and non-plastic based on ASTM D4318 (2010). Figure 2.1 shows the gradation of the sand using the tests following ASTM D1140 (2017) and ASTM D421 (2007), respectively.

Kaolin for this blend is an Edgar Plastic Kaolin (EPK) clay from Edgar Minerals in Florida. This fine material has a mean particle size of 1.36 microns; it is extremely fine and is delivered in 50-pound (23-kg) bags. Specific gravity of the kaolin is 2.65, its pH is 5.5 to 6.5, and its water retention is 25% (Edgar Minerals, 2018). Figure 2.2 shows the Atterberg limits (ASTM D4318, 2010) of the kaolin materials from different pallets received, including the Liquid Limit (LL) of approximately 60 and the Plasticity Index (PI) of approximately 25.

These two components for the subgrade were blended at a dry weight ratio of 25% kaolin to 75% sand. Once the subgrade was mixed uniformly, its index properties were obtained in the soil testing laboratory. Wet sieve analysis was performed on the mixed material to determine its gradation as displayed in Figure 2.3. Subgrade samples were compacted in 150 mm (6 in.) standard Proctor molds following ASTM D698 (2012). These samples were used to perform California Bearing Ratio (CBR) tests (ASTM D1883, 2016) as well as hand-held vane shear tests (ASTM D4648, 2016). Unconfined Compression (UC) samples were also prepared and tested for their unconfined compressive strengths (ASTM D2166, 2016). Figure 2.4, Figure 2.5, and Figure 2.6 show these test results. The hand-held vane shear (VS) strength in kPa was approximately equal to 30 times the subgrade CBR value. The UC shear strength values are approximately half those obtained using the hand-held vane shear tests.

The shear strength values of the subgrade obtained in the large box were similar to those obtained using the hand-held vane shear tests in the Proctor molds, as will be discussed in subsequent sections. This study used the target CBR values of 2% (i.e., weak subgrade) and 5% (intermediate subgrade) for the subgrade in the large box testing. These CBR values were targeted according to the moisture content-CBR relationship as shown in Figure 2.5 to select the approximate moisture contents to prepare subgrade soils. It should be noted that the purpose of Figure 2.5 was not to determine the maximum dry density and its corresponding optimum moisture content.

In addition to the vane shear tests, the dynamic cone penetrometer (DCP) tests (ASTM D7380, 2008) were conducted for quality control of the subgrade and the granular base in the large box tests. The correlation between the DCP penetration index and the CBR value provided in ASTM D7380 (2008) was used to estimate the CBR values of the subgrade and the granular base.

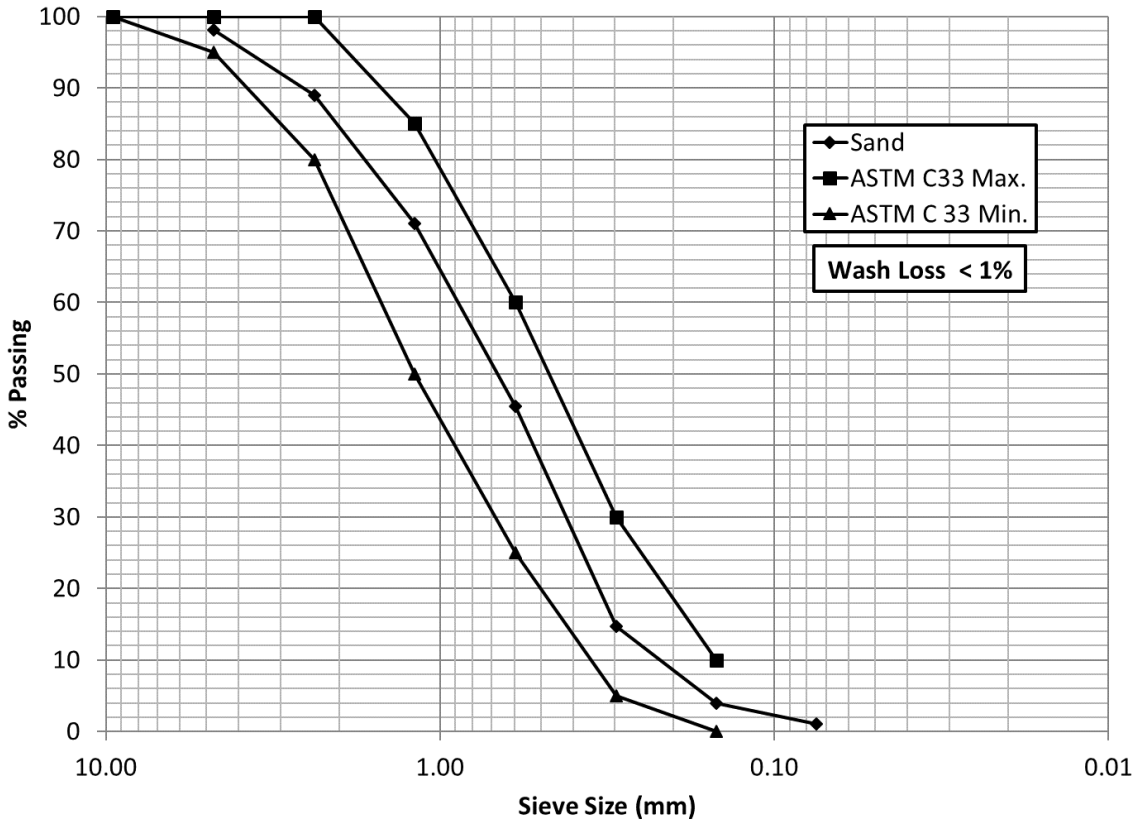

Figure 2.1: As-received Gradation of ASTM C 33 Sand for Subgrade Blend

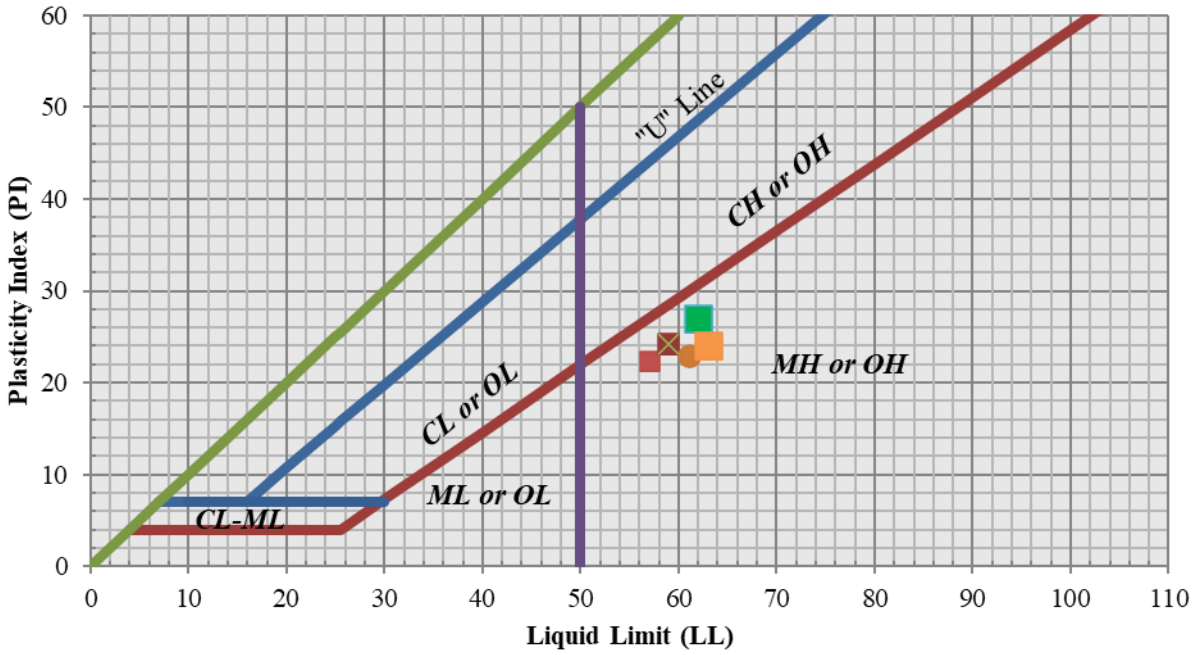

Figure 2.2: Atterberg Limits of EPK Kaolin as Received from Edgar Materials

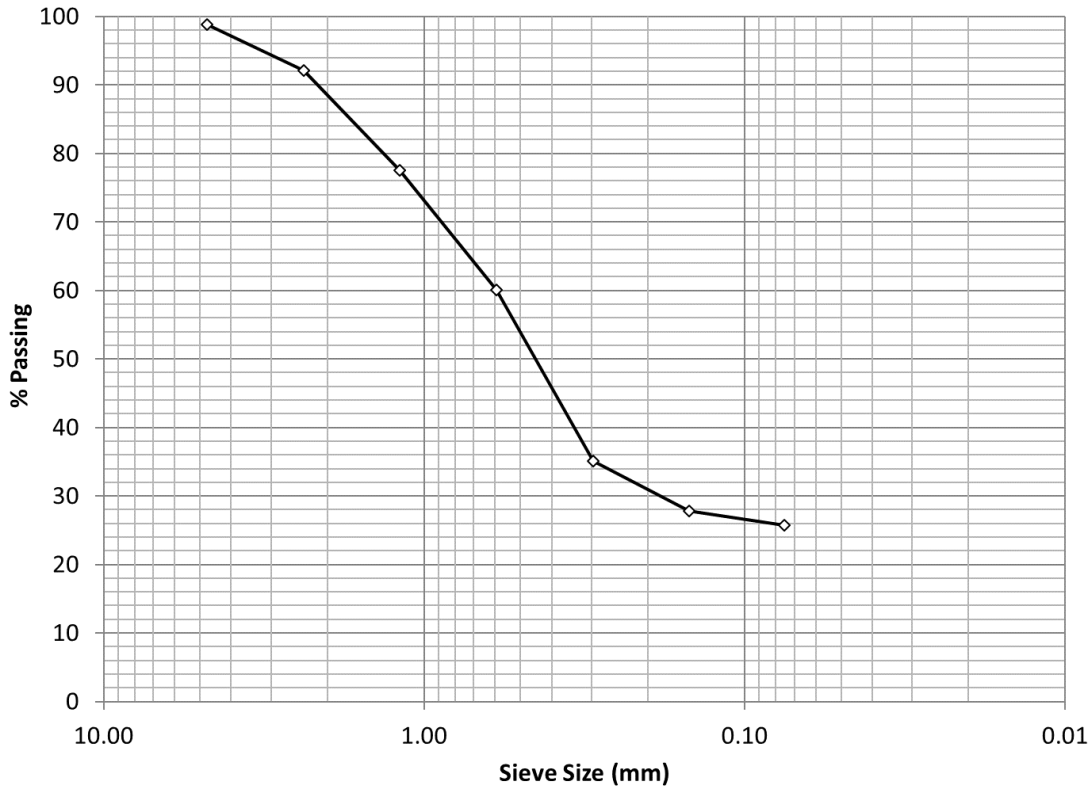

Figure 2.3: Subgrade Grab Sample Gradations from Stockpile

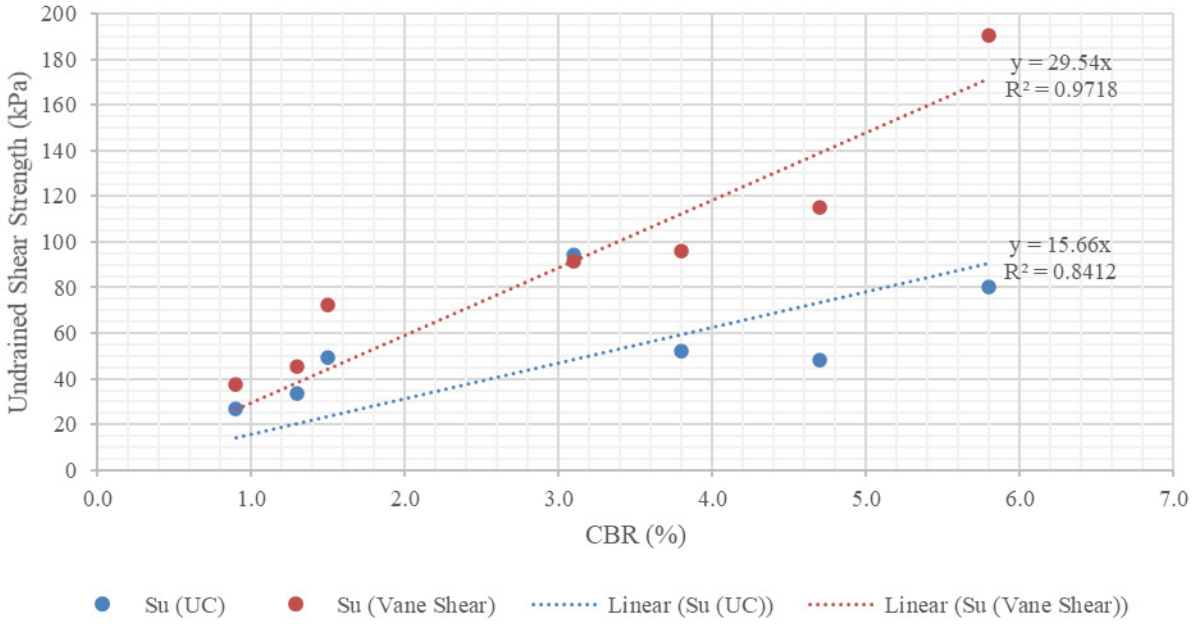

Figure 2.4: Subgrade Laboratory Undrained Shear Strength vs. CBR

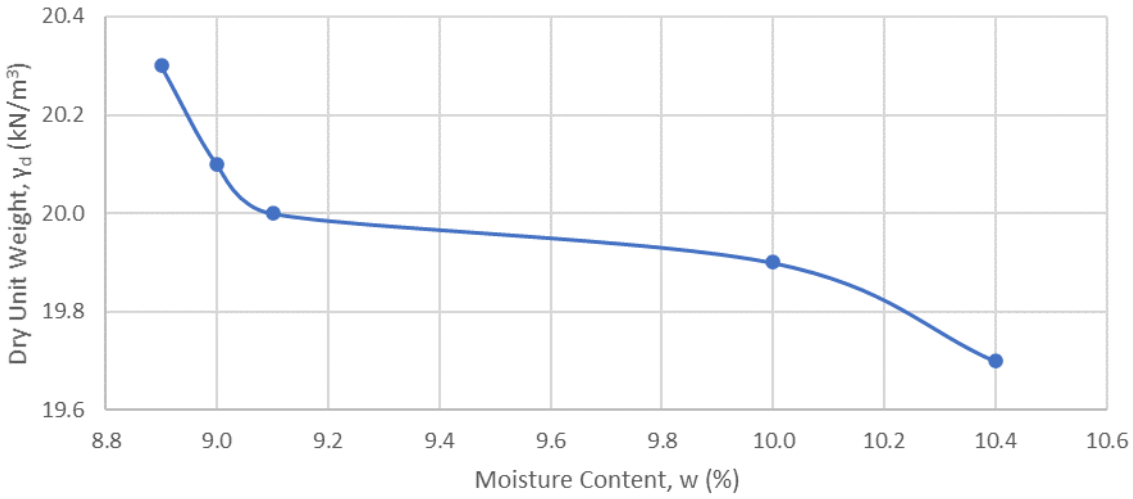

Figure 2.5: Subgrade Standard Proctor Unit Weight vs. Moisture Content

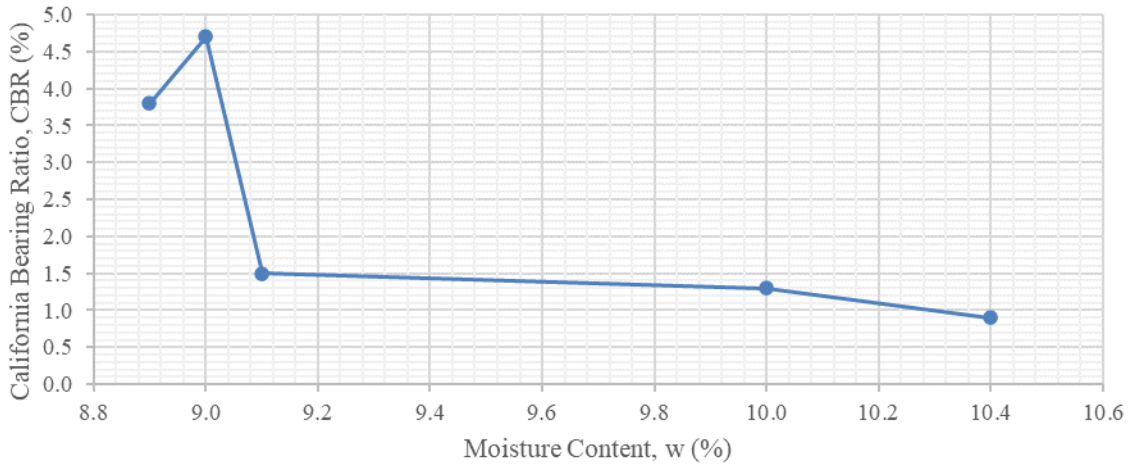

Figure 2.6: Subgrade Moisture Content vs. CBR from Standard Proctor Mold

2.1.2 Virgin Granular Base (VGB)

Granular base material in this study conformed to the KDOT (2015) specification for granular base Section 1106, 15-ER-1-R19. This material consisted of crushed limestone from a local aggregate source near Lawrence in Kansas. Sieve analysis (ASTM D1140, 2017; ASTM D421, 2007) was conducted upon receipt of the base course material and during testing to assure the specification was met. Standard Proctor tests (ASTM D698, 2012) were conducted to obtain the compaction curve of VGB as shown in Figure 2.8, in which the unit weight corresponding to 95% relative compaction was determined for the large box testing. The optimum moisture content

and its corresponding maximum dry unit weight of the VGB were 7.1% and 21.2 kN/m^3 (135 pcf), respectively. The unit weight corresponding to 95% relative compaction was 20.2 kN/m^3 (128 pcf). Relative compaction of 95% or higher was obtained in the large box tests within the moisture content range of 6.7% to 7.5%.

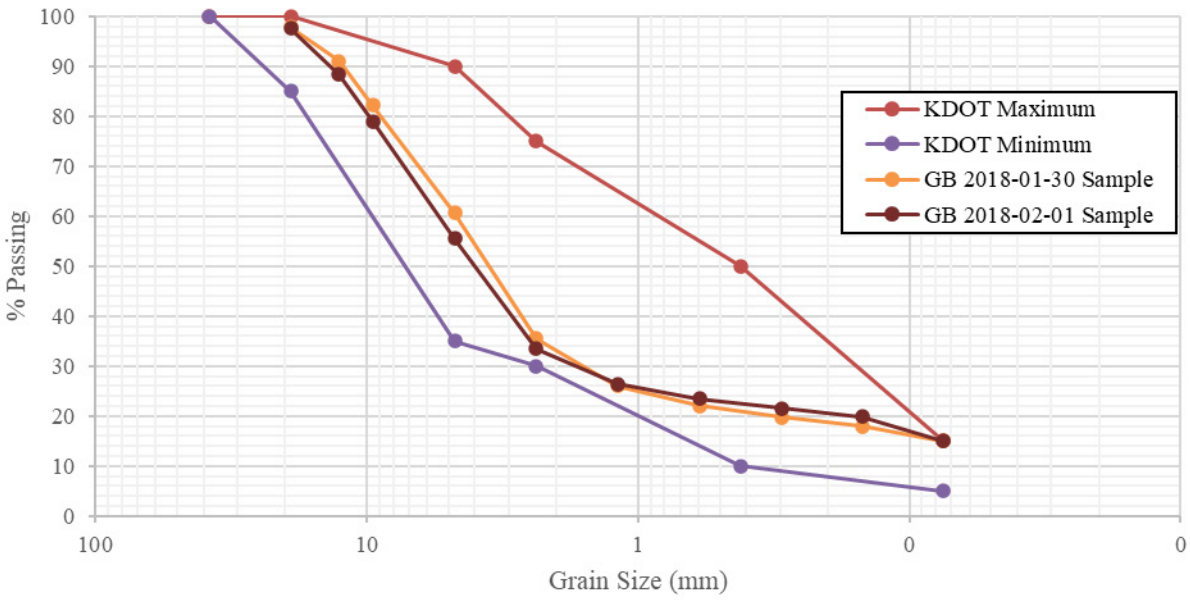

Figure 2.7: Grain-size Distribution of Virgin Granular Base (VGB) and KDOT Specification

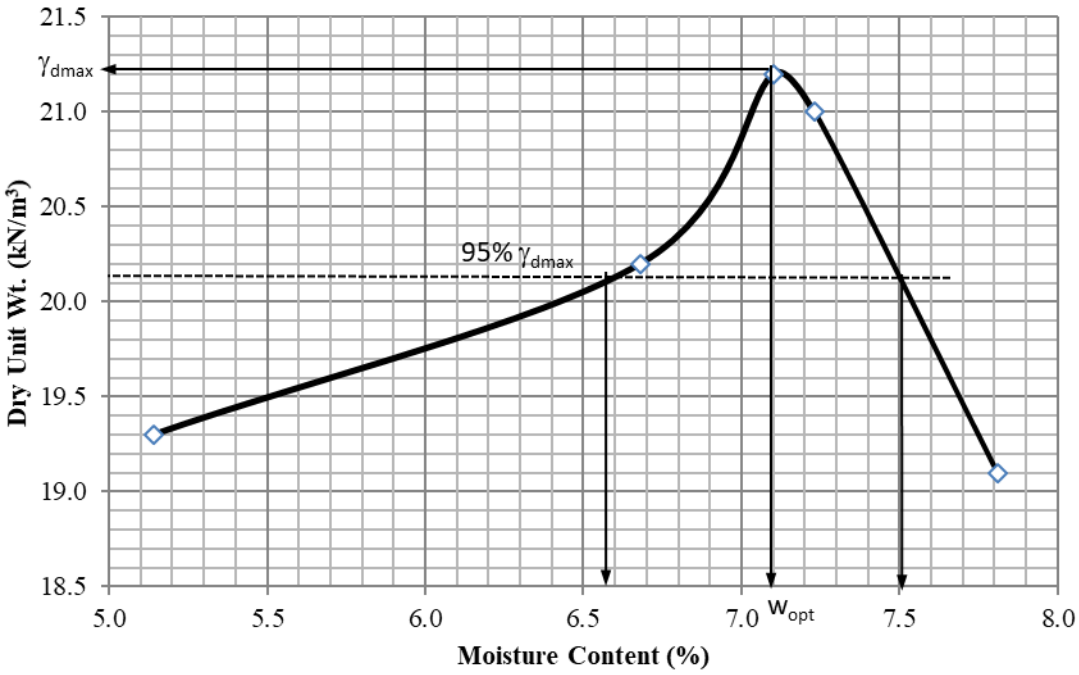

Figure 2.8: Moisture-Density Curve of Virgin Granular Base (VGB)

2.1.3 Recycled Concrete Aggregate (RCA)

Recycled concrete aggregate (RCA) was sourced from a local producer in Lawrence, Kansas. However, the source or location of the concrete pavement crushed into RCA is unknown; inherent variability is part of using an RCA material for construction, especially if the material source is unknown. This RCA material was determined as non-plastic (NP) because the sample changed from a granular state to continually sliding in the Casagrande cup at increasing moisture content during the Atterberg limit tests (ASTM D4318, 2010). Sieve analysis shows that the gradation meets the KDOT specification for granular base (see Figure 2.9). The compaction curve from the Standard Proctor tests (ASTM D698, 2012) in Figure 2.10 shows that the maximum unit weight and its corresponding optimum moisture content were 17.9 kN/m^3 (114 pcf) and 12.8%, respectively. Relative compaction of 95% was achieved at the dry unit weight of 17.0 kN/m^3 (108 pcf) and the moisture contents of 9.7% (dry side) and 17.5% (wet side). As compared with the VGB, the moisture content range for the desired unit weight indicates that the RCA is a more absorptive material and is less sensitive to changes in moisture content.

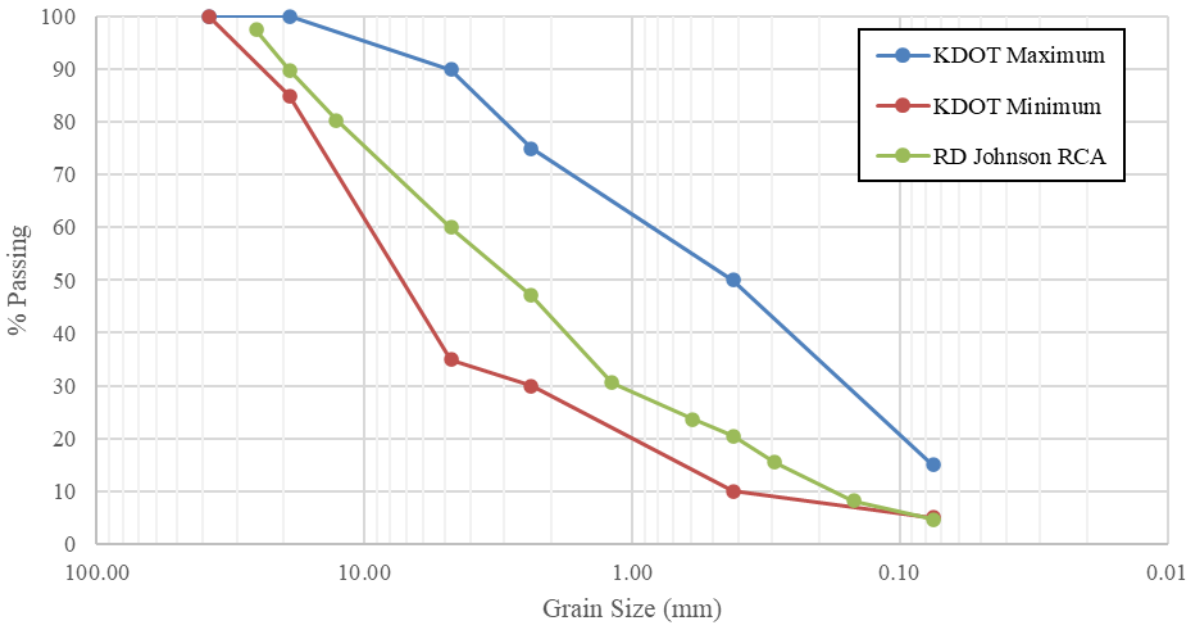

Figure 2.9: Grain Size Distribution of RCA vs. KDOT Granular Base Specification

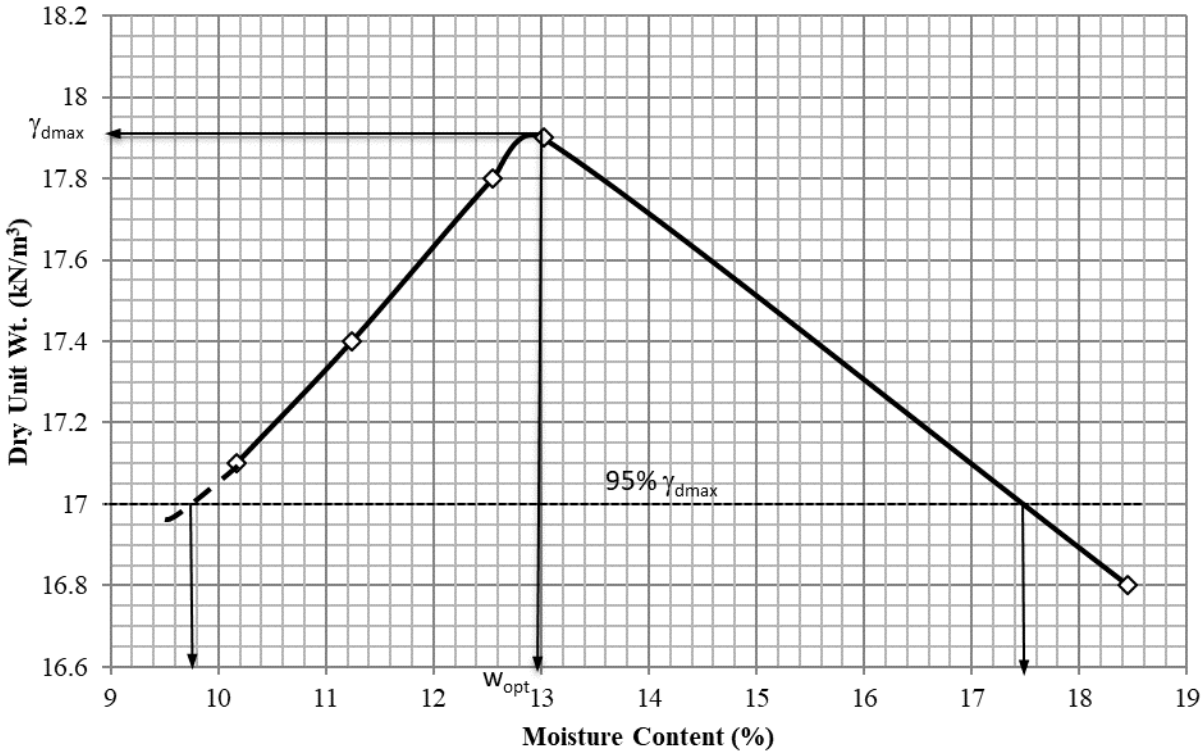

Figure 2.10: Moisture-Unit Weight Curve of RCA

2.1.4 Geosynthetics

Geosynthetics for this study were chosen from the KDOT list of pre-qualified materials (KDOT, 2018). This selection ensures that the large box testing is applicable to current practice in KDOT. Figure 2.11, Figure 2.12, and Figure 2.13 show nonwoven geotextile (NW), woven geotextile (W), and triaxial geogrid (GG) used in the large box testing. Table 2.1, Table 2.2, and Table 2.3 list the properties of each geosynthetic used.

Figure 2.11: Nonwoven geotextile

Table 2.1: Nonwoven Geotextile Properties

Geosynthetic Type	Non-Woven Geotextile (NW)
KDOT Pre-Qualified Material	Yes
Grab Strength (N)	710
Tear Strength (N)	270
Puncture Strength (N)	420
Burst Strength (kPa)	2,100
Permittivity (s^{-1})	1.4
AOS (mm)	0.212
UV Stability (%)	70

Figure 2.12: Woven geotextile

Table 2.2: Woven Geotextile Properties

Geosynthetic Type	Woven Geotextile (W)
KDOT Pre-Qualified Material	Yes
Tensile Strength (kN/m) @ 2% Strain	14
Tensile Strength (kN/m) @ 5% Strain	35
Tensile Strength (kN/m) @ 10% Strain	70
Tensile Strength (kN/m) ultimate	70
Permittivity (s^{-1})	0.4
AOS (mm)	0.600
UV Stability (%)	80

Figure 2.13: Triaxial Geogrid (with VGB)

Table 2.3: Triaxial Geogrid Properties

Geosynthetic Type	Triaxial Geogrid (GG)
KDOT Pre-Qualified Material	Yes
Junction Efficiency	93%
Radial Stiffness (kN/m @ 5% strain)	225
Rib Pitch (mm)	40
Mid-Rib Depth (mm)	1.2
Mid-rib Width (mm)	1.1
UV Stability (%)	70

2.1.5 Concrete

A commercially available, quick-cure concrete mix was selected for reducing curing time as well as minimizing any human factors in mix design. Typical concrete pavement has a 28-day unconfined compressive strength of 21 MPa (3,000 psi) (Huang, 2004). To accelerate testing by achieving this minimum strength in 7 days instead of 28 days, the commercial concrete mix was selected that meets this minimum strength (see Figure 2.14). Water was added according to the product instructions at 2 liters (0.5 gallons) per 27.2-kg (60-lb) bag of concrete to yield 0.014 m^3 (0.5 ft^3) per bag. Concrete and water were mixed to uniformity, poured into a grease- and foam-lined wooden formwork inside the large box, and followed by hand-tamping and hand-smoothing.

Two samples were taken from the mixed concrete during pouring and cured in a humidity-controlled room for eight days to confirm the unconfined compressive strength. Compressive strength of this concrete was measured at an average of 28.5 MPa (4,100 psi), which is higher than the rated strength from the manufacturer (see Figure 2.14). Using the American Concrete Institute (ACI) recommendations, the tensile strength is roughly 10% f'_c of standard-strength concrete at 2.85 MPa (410 psi) and the modulus of elasticity E_c is 25.3 GPa (3.7 x 10^6 psi) based on 57,000 multiplied by the square root of f'_c in psi (Oluokun, Burdette, & Deatherage, 1991).

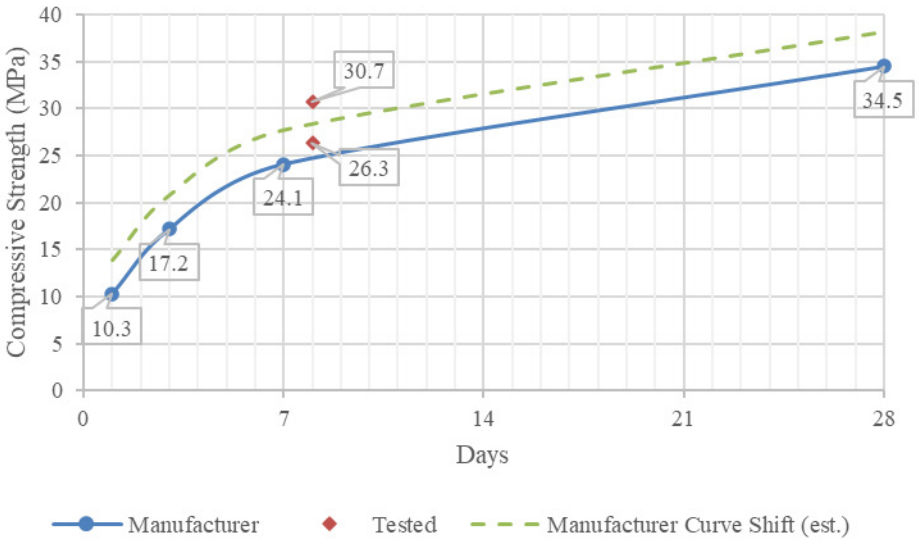

Figure 2.14: Concrete Compressive Strength with Curing Time

2.2 Preparation and Testing of Road Sections

Figure 2.15 depicts an unpaved road section for cyclic plate loading tests in the large box, which includes subgrade, geosynthetic if used, base course, a loading plate, an actuator, and instrumentation (earth pressure cells shown as an example). A road section with a concrete slab will be presented later. The following sections detail how a test section was constructed.

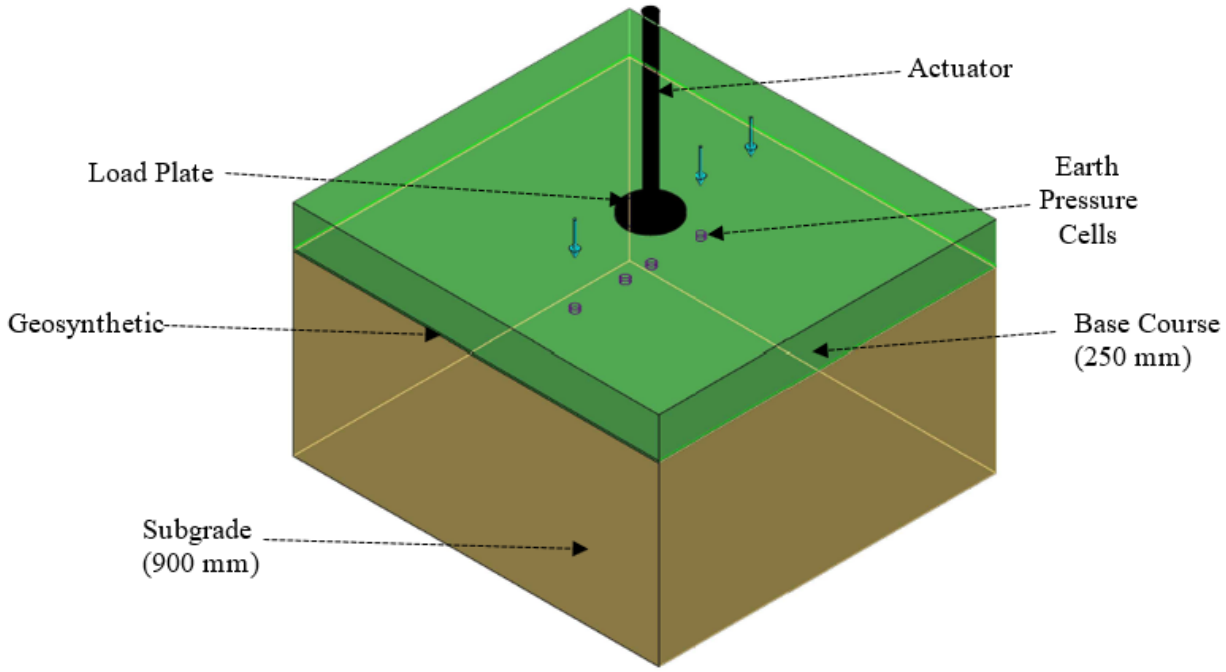

Figure 2.15: A Typical Unpaved Road Section for Cyclic Plate Loading Test in the Large Box

2.2.1 Preparation of Subgrade

Subgrade was blended outdoors to the target moisture content first based on the CBR-moisture content curve in Figure 2.6 and then adjusted based on the DCP test result after the subgrade was placed in the box (e.g., the moisture content was increased to 9.76% to achieve 2% CBR). Once the target moisture content was confirmed, the subgrade soil for each lift was brought into the box using the skid steer, roughly leveled by hand tools, and then compacted using a vibratory compactor. The subgrade in each test section was formed by six 150-mm lifts of subgrade soil. Prior to placement, the total subgrade thickness of 900 mm from the base of the box was divided equally into six layers (150 mm each layer) and marked along the inside of the large box. The density of the subgrade soil was controlled by the weight-volume method (i.e., the calculated amount of soil based on the weight required to fill the box volume was placed and compacted in the box to the level of each lift to ensure the soil weight divided by its volume equal to the desired soil density). Quality control for the subgrade strength was performed on each lift using a hand-held vane shear device (see Figure 2.4), but quality assurance and determination of the section

subgrade CBR were done by DCP tests. Once the subgrade quality was assured, earth pressure cells (EPC) were installed on the surface of the subgrade.

2.2.2 Placement of Geosynthetic

When a geosynthetic was part of the test section, it was placed at the top of the subgrade after the installation of earth pressure cells. To assure adequate coverage and anchorage, the geosynthetic was cut so that approximately 100 mm additional material was left on each of the four sides. The geosynthetic layer (nonwoven geotextile, woven geotextile, or triaxial geogrid) was gently tensioned by holding its corners to the box edges and smoothing by hand. The geosynthetic was then secured in each corner through railroad spikes hammered through the geosynthetic into the subgrade.

2.2.3 Placement of Base Course

Base course material was placed and then compacted in two lifts in place atop the geosynthetic (or subgrade in the case of a control section). Prior to the placement, vertical distances of 250 mm from top of subgrade or geosynthetic were marked along the inside of the large box. Each lift was 125 mm in thickness, creating a 250-mm-thick base course section over weak subgrade. Aggregate material was prepared to the optimum moisture content outside the lab, then brought in via a skid steer and hand-leveled roughly. The same vibratory compactor was used to compact each lift. The aggregate surface was checked for level beneath the loading plate to assure full contact with the load plate. Quality assurance was performed for dry unit weight of the aggregate using the sand cone test (ASTM D1556, 2015) to assure at least 95% relative compaction. Thickness of the section was also confirmed by direct measurement after the test and the large box panels removed, as displayed in Figure 2.16.

Figure 2.16: Direct Measurement of Base Course Thickness after the Test

2.2.4 Concrete Slabs

When present, two concrete slabs of 150 mm thick with a 12.5-mm-wide joint were poured inside the large box atop the compacted base course. Figure 2.17 through Figure 2.20 depict the layout of the large box with the concrete slabs. The slabs were poured such that the 150-mm loading plate applied a load onto the corner of one slab. Two rebar lifting hooks were poured in the center of each slab to help with extraction after the test (see Figure 2.21 and Figure 2.22). Figure 2.21 displays the framework and the first partially poured concrete slab. Concrete cured for seven days beneath a wetted burlap prior to applying the first load sequence. Aggregate was filled level with the slabs on one side to simulate an unpaved shoulder condition and hand-tamped before loading. After the first load sequence at Day 7 of curing, approximately 300 liters (79 gallons) of water were applied to the test section through a sprinkler system (see Figure 2.23). The wetted section was left overnight, and the second load sequence was applied at Day 8. Wetting the test section was to simulate rainfall and to evaluate its effect on pavement performance.

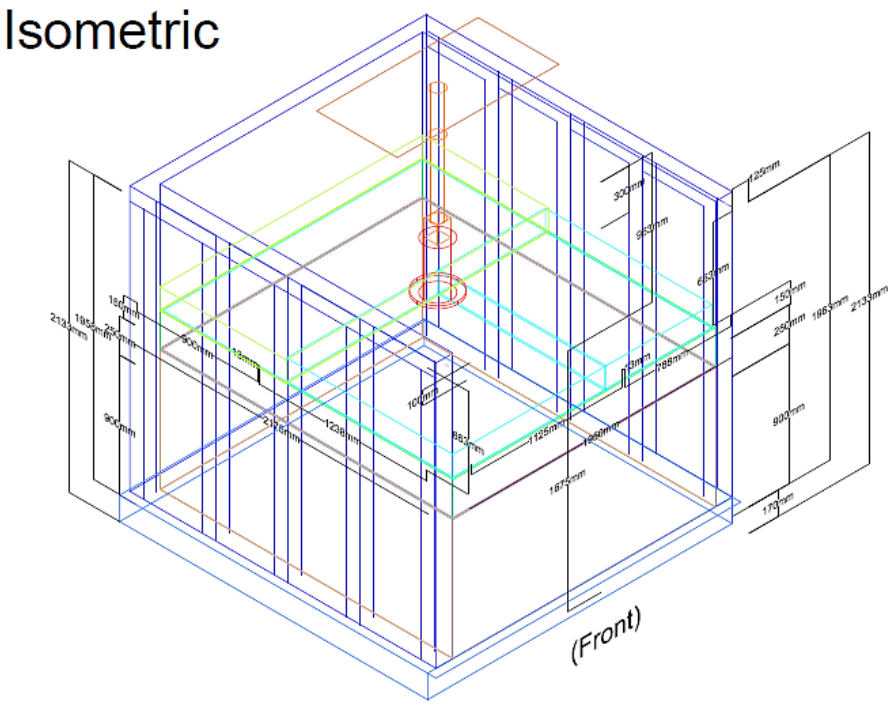

Figure 2.17: Large Box Layout with Concrete Slabs (Isometric View)

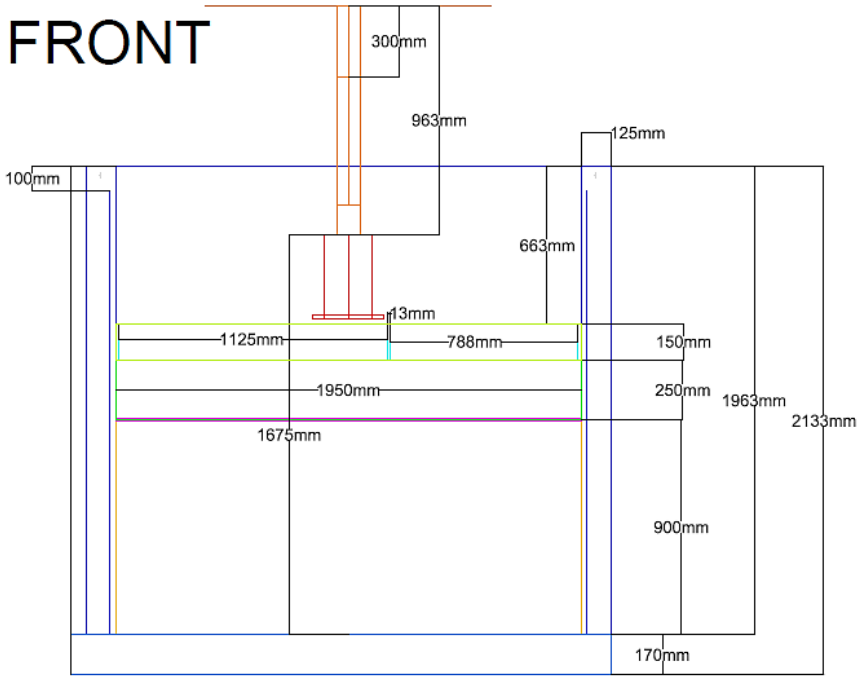

Figure 2.18: Large Box Layout with Concrete Slabs (Front View)

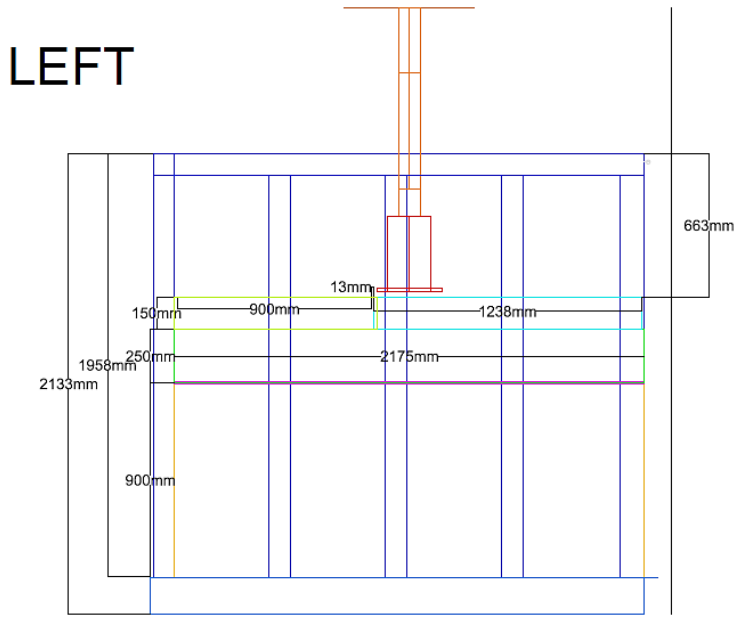

Figure 2.19: Large Box Layout with Concrete Slabs (Left View)

TOP

Total Concrete Slab Volume = 0.37 cubic meters per pour

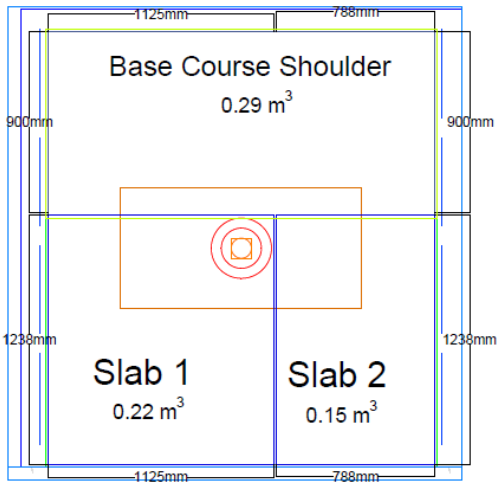

Figure 2.20: Large Box Layout with Concrete Slabs (Top View)

Figure 2.21: Concrete Slab during Pour and Compaction

Figure 2.22: Concrete Slabs after Pour with An Overlying Burlap to Preserve Moisture

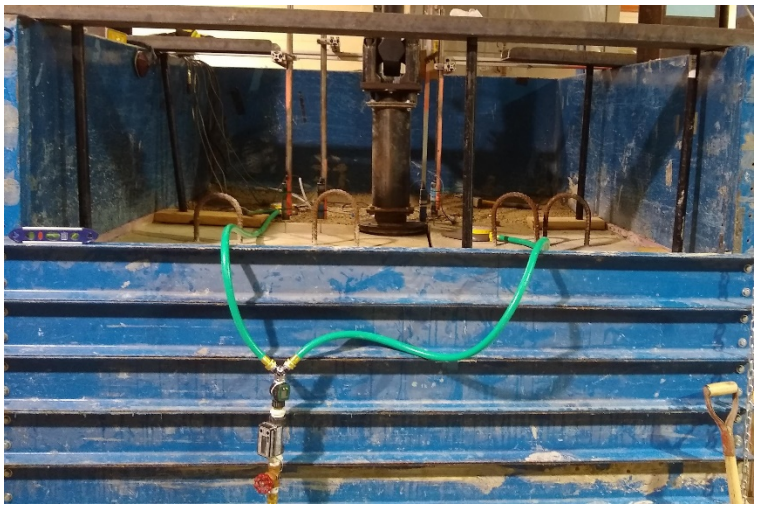

Figure 2.23: Sprinklers for Applying Water to Simulate Rainfall

2.2.5 Installation of Instrumentation

To better evaluate performance of the base course section, several measurements were recorded at the surface of the base course (or concrete pavement) and at the surface of the subgrade (i.e., the interface between the base and the subgrade). Once the subgrade quality was assured, 100-mm-diameter earth pressure cells (EPC) were installed on the surface of the subgrade at 0-mm, 150-mm, 300-mm, and 450-mm offsets from the center of the loading plate. Readings of earth pressure cells were taken every 0.1 second.

Displacement transducers were placed on the surface of each test section. For the unpaved sections (Figure 2.24), transducers measured the displacements on the plate, at twice the radius, R, from the center, and at thrice the radius from the center. For the paved sections (Figure 2.25), transducers were placed at the loaded corner of the slab, at twice and thrice the radius of the plate from the center of the plate along the diagonal of the loaded slab (2R and 3R), and at the load-adjacent edge of the non-loaded slab. From these measurements, the distance from the center of the load to the point of rotation, L, (i.e., $\delta_L = 0$), the loaded corner deflection, δ_c, and the deflections at 2R and 3R, δ_{2R} and δ_{3R}, can be found (Figure 2.26). Figure 2.24, Figure 2.25, and Figure 2.27 show the fully assembled test sections.

Figure 2.24: Displacement Transducers on the Surface of Base Course in An Unpaved Road Test

Figure 2.25: Displacement Transducers on a Concrete Slab in a Paved Road Test

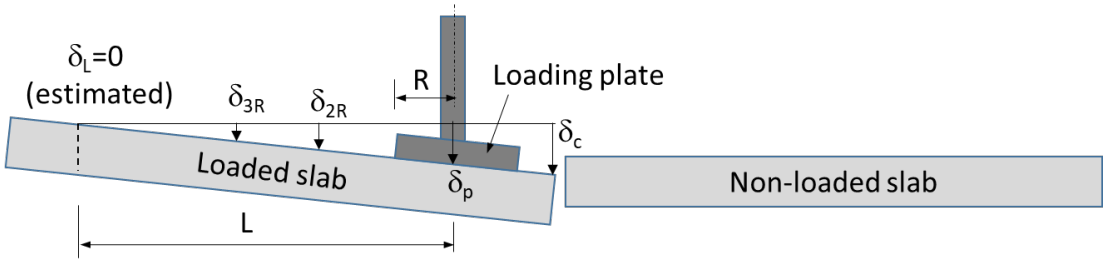

Note: z_c, z_{2R}, and z_{3R} were the displacements measured by the transducers at these locations.

Figure 2.26: Illustration of Concrete Pavement Test Setup with Instrumentation

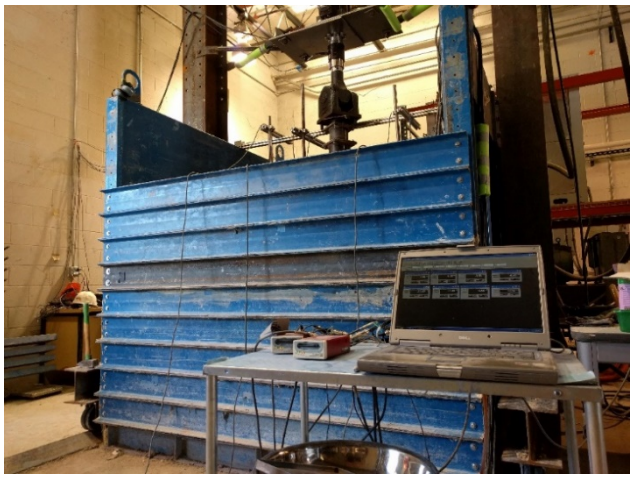

Figure 2.27: Front View of the Test Box and Setup

2.3 Load Sequence

2.3.1 Unpaved Road Sections

2.3.1.1 Static Load Test

Once the test section was constructed, quality of construction was assured, and the load plate was leveled, a static load sequence was applied to the test section surface through the loading plate. This loading sequence served a couple of purposes. AASHTO (1993) states that the static loading method should be used to determine the k-value of a uniform subgrade, but this method may not yield consistent or valid results for layered pavement sections. Running this sequence in this study was to verify the recommendation outlined in the AASHTO (1993) guide. This static sequence also provides a seating preload identified in other studies. However, there has not been a consistently designated method of preload, whether it should be static or cyclic loading. Therefore, a method similar to that used in a triaxial test to preload a sample with static loads before applying a cyclic load sequence was adopted in this study. Table 2.4 lists load increments for the static sequence. The load was applied by the actuator through the loading plate, and the displacement and its corresponding applied load were monitored by the sensors in the actuator. The applied load was maintained until the displacement was 0.03 mm per minute for three consecutive minutes. Once the maximum desired load (6.75 kN or 1520 lb) was reached and the displacement was stabilized, unloading was performed in several stages to zero to prepare for cyclic loading.

Table 2.4: Static Load Test Sequence

Stage No.	Target Load (kN)	Stage No.	Target Load (kN)
1	0.00	9	3.75
2	1.50	10	4.50
3	3.00	11	5.25
4	0.00	12	6.00
5	0.75	13	6.75
6	1.50	14	4.00
7	2.25	15	2.00
8	3.00	16	0.02

Note: 1 kN = 225 lb

2.3.1.2 Cyclic Load Test

After the section was preloaded and then unloaded, an automated program activated the actuator to apply the cyclic load sequence. Table 2.5 details load increments and number of cycles for each load stage. The waveform for each 1.3-second load cycle (Figure 2.28) included a ramp up to the desired load for 0.3 second, maintenance of the load for 0.2 second, unload down to 0.02 kN (4.5 lb) over 0.3 second, and maintenance of the unloaded state for 0.5 second. The reason for maintaining a small load was to prevent the loading plate from losing contact with the base course and applying an impact load instead of pulsing. In the unpaved road tests, displacement of the plate was limited to approximately 38 mm (1.5 in.) while in the concrete pavement tests, displacement was limited to 13 mm (0.5 in.) because the concrete slab could not tolerate large deformation. Load magnitudes used in this study reflect the stress increments of the resilient modulus tests (AASHTO T 307, 2017). The contact pressure was calculated by dividing the applied load by the plate contact area.

Table 2.5: Cyclic Load Sequence

Stage No.	Applied Load (kN)	Contact Pressure (kPa)	No. Cycles	Stage No.	Applied Load (kN)	Contact Pressure (kPa)	No. Cycles
1	1.0	14	200	6	7.5	103	2,000
2	2.0	28	200	7	10.1	138	2,000
3	3.0	41	200	8	15.1	207	2,000
4	4.0	55	200	9	20.1	276	2,000
5	5.0	69	200	10	25.2	345	2,000
				11	30.2	414	2,000

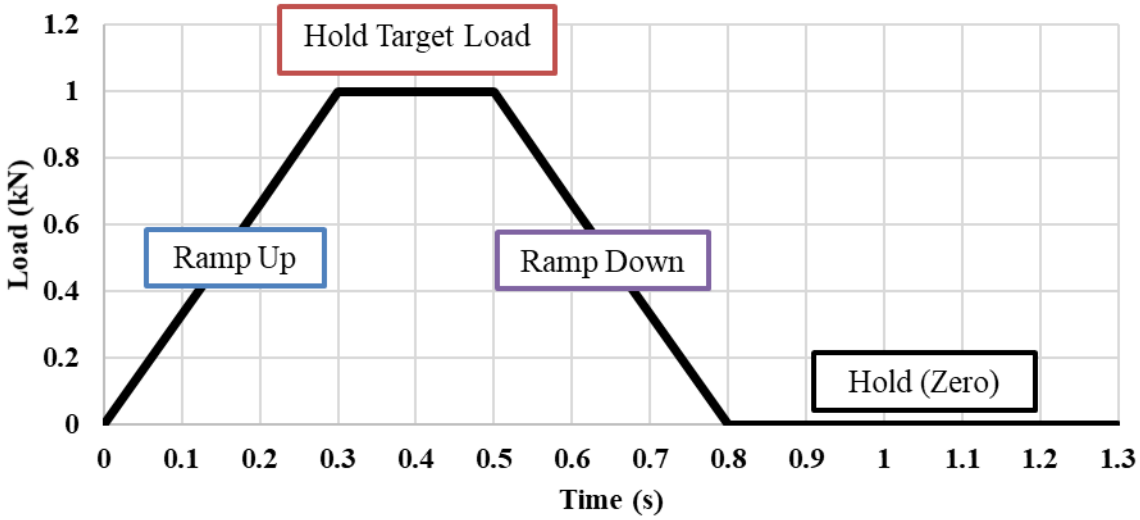

Figure 2.28: Single-Cycle Load Waveform

The test results showed permanent deformations were minimal at the small number of low-intensity cycles, typically less than 10 mm (0.4 in.) (in some cases less than 5 mm or 0.2 in.). Surface imperfections in the base course did not have an opportunity to be smoothed with so few cycles, so no consistent pattern of behavior could be determined. It was decided to increase the number of load cycles and stages to instigate more deformation. A trial test with VGB and woven geotextile was conducted using an initial alternate load sequence that allowed the final stage of cycles to run with a target 38 mm (1.5 in.) permanent deformation. Unfortunately, 3,000 cycles was not enough to cause the desired permanent deformation (i.e., only 3.75 mm). The sequence was again modified to the current load sequence (Table 2.5) in order to observe any effects of load magnitude by reaching at least 25 mm of permanent deformation due to cyclic loading. Trials were

also conducted on unpaved road tests with 100-mm-thick aggregates over 5% CBR subgrade, which generated very small and inconsistent surface deformations; therefore, 2% CBR subgrade was selected for further tests.

2.3.2 Concrete Pavement Sections

For the test sections with a concrete slab atop the base course and subgrade, a single load magnitude was applied at Day 7 after the concrete was poured and at Day 8 after the test section was subjected to rainfall. Tests "A" and "B" refer to the initial or pre-rainfall (Day 7) and post-rainfall (Day 8) tests, respectively. The applied load of 40 kN (9 kip) corresponds to the equivalent single wheel load (ESWL) (AASHTO, 1993). No static preloading was performed for the concrete pavement sections because the concrete slab was rigid and possible irregularities in the underlying base course were removed through the installation and compaction of overlying concrete. Table 2.6 provides the load sequences for the concrete pavement test sections.

Table 2.6: Applied Loads for Concrete Pavement Sections

Stage No.	Applied Load (kN)	Contact Pressure (kPa)	No. of Cycles
A	40	550	15,000
B	40	550	15,000

Note: 40 kN = 9 kip and 550 kPa = 80 psi.

2.4 Test Summary

Table 2.7 summarizes the conditions for the cyclic plate loading tests in the large box without any concrete pavement. Table 2.8 summarizes the conditions for the concrete pavement test sections. The CBR values listed in these tables come from DCP test results taken prior to testing in unpaved road sections or concrete installation in concrete paved sections.

Table 2.7: Unpaved Test Matrix

Base Course Material	Base Course Stabilization	SG CBR (%)	BC CBR (%)
VGB	W	2.2	11.6
RCA	W	2.0	13.4
RCA	NONE	2.1	13.1
VGB	NONE	1.9	12.4
RCA	GG	2.0	14.9
VGB	NW	2.2	13.0
RCA	NW	2.0	16.3
VGB	GG	2.1	14.5
VGB	NW	2.9	14.0
RCA	GG over NW	2.0	17.2
VGB	GG over NW	1.9	14.9

Table 2.8: Concrete Pavement Test Matrix

Base Course Material	Base Course Stabilization	SG CBR (%)	BC CBR (%)
VGB	NONE	2.2	8.5
VGB	NW	2.2	10.8
RCA	NW	2.0	15.2

Chapter 3: Unpaved Road Test Results and Analysis

3.1 Introduction

Unpaved road tests were conducted to evaluate the properties of the granular bases over the subgrade with or without a geosynthetic before the placement of a concrete slab. These properties are often needed for design of concrete pavements. This chapter will discuss the unpaved road test results and then determine and analyze their properties.

3.2 Static Preload Deformations

Prior to cyclic loading, each unpaved test section was statically loaded to 6.75 kN (1.52 kips) to remove any surface imperfections. This deformation was minimal, as displayed in Table 3.1. In general, the RCA sections consistently exhibited less deformation than the VGB sections during preloading. These data only show the initial conditions and should not be used to evaluate the performance of each test section.

Table 3.1: Deformations of Test Sections Induced by Initial Static Loads

Aggregate	Geosynthetic	Deformation (mm)
VGB	Control	2.7
VGB	NW	1.7
VGB	W	2.1
VGB	GG	1.8
VGB	GG/NW	3.3
RCA	Control	1.4
RCA	NW	1.3
RCA	W	1.0
RCA	GG	1.6
RCA	GG/NW	1.2

3.3 Cyclic Deformations

Under cyclic loading, each load cycle included both resilient and permanent deformations. Figure 3.1 shows the deformations of the test sections during cyclic loading, in which the minimum values depict the accumulated permanent deformations at the loading plate while the thickness of each band (i.e., the maximum deformation minus the permanent deformation under each load cycle) displays the resilient deformation.

Figure 3.2 shows the accumulated permanent deformations induced by the applied loads. As testing was terminated at roughly 38 mm (1.5 in.), several of the VGB sections were subjected to fewer load increments. In the earlier stages with lower load magnitudes, the differences in the permanent deformations are minimal. Within the first 1,000 load cycles completed in the first five sequences (up to 69 kPa), all the load-displacement curves are nearly linear, and their differences are all less than 1 mm. Later load sequences show more differences in the measured permanent deformations. In general, the test sections with RCA exhibited less permanent deformation with the increase of both load magnitude and number of cycles than those with VGB.

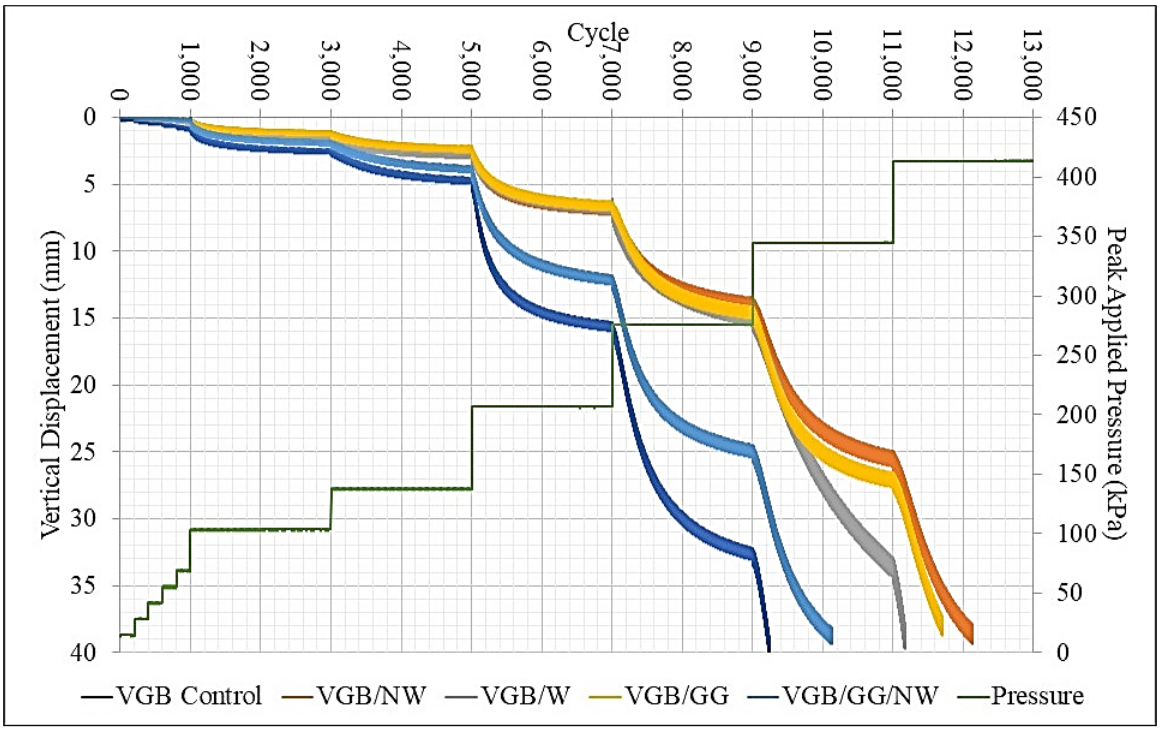

(a) VGB Base Course

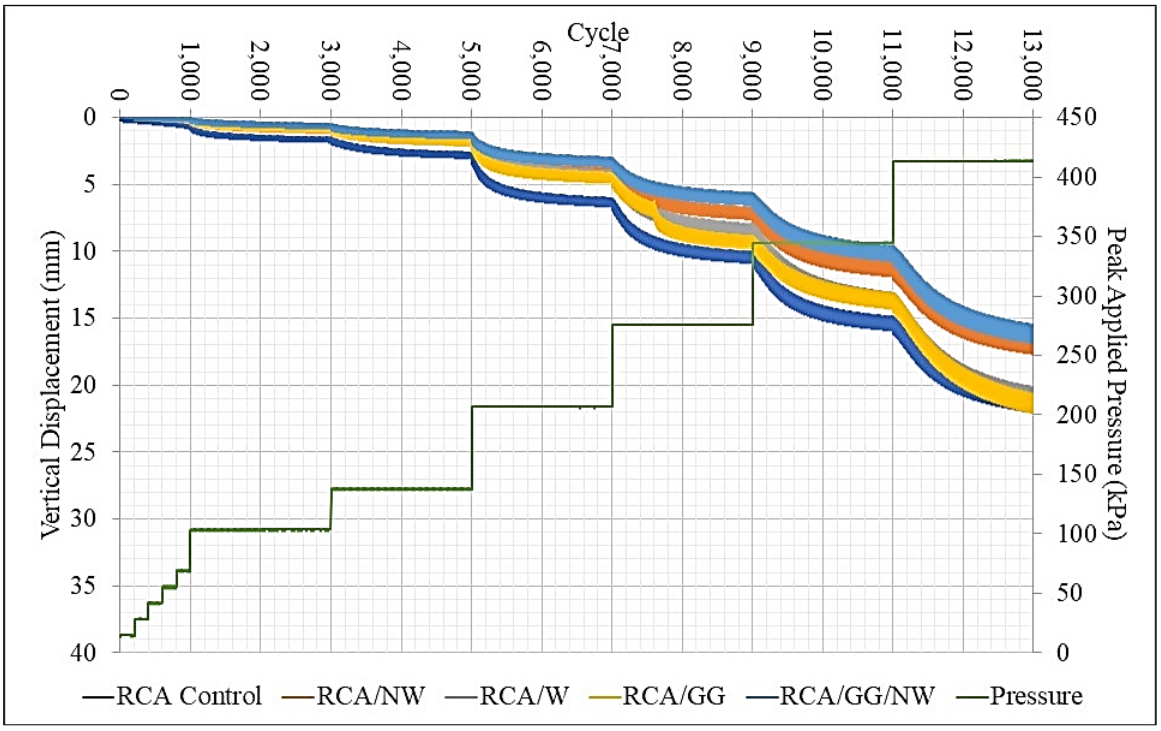

(b) RCA Base Course

Figure 3.1: Displacements by Loads Cycles for Unpaved Road Sections

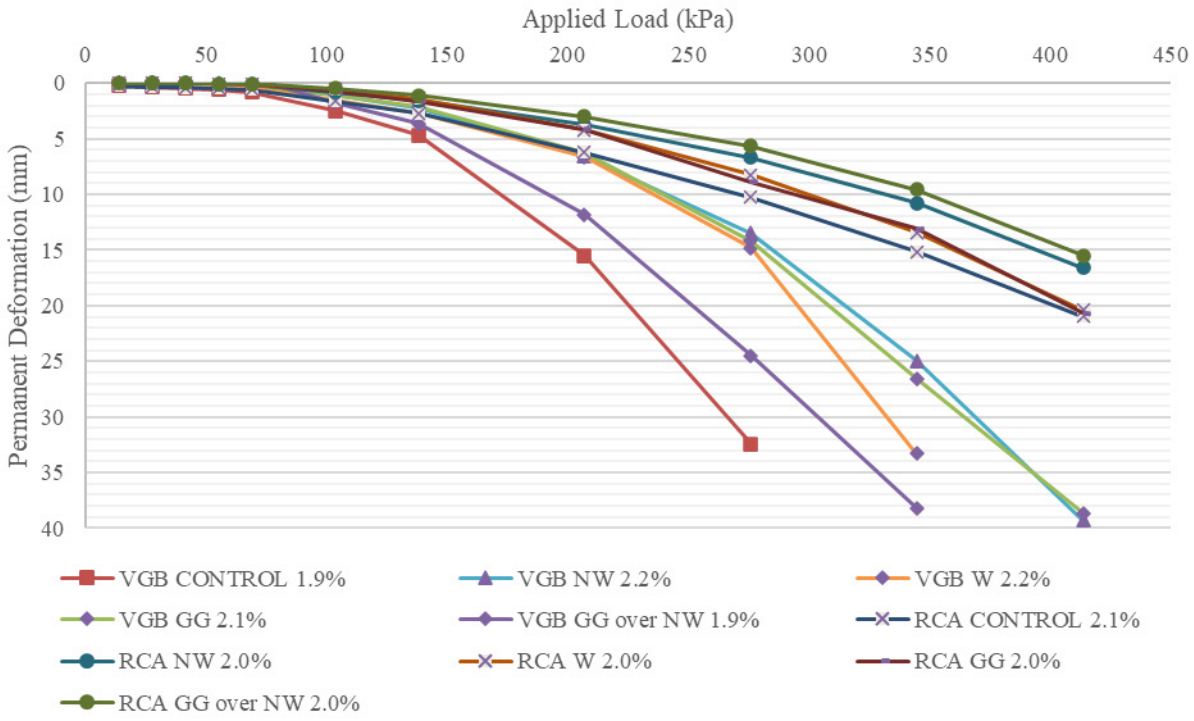

Figure 3.2: Accumulated Permanent Deformations of Unpaved Road Sections by Load Sequence

Table 3.2 provides the accumulated permanent deformations for the unpaved road sections up to Load Sequence No. 9 (i.e., 20.1 kN or 276 kPa) (4.5 kips or 40 psi). In general, the control sections had the largest permanent deformations. The test sections with geosynthetics had smaller permanent deformations than the control sections and similar permanent deformations with each other. Given the similar performance, no geosynthetic option was the "best" option in terms of reduced deformation, and the magnitude in the permanent deformation reduction was not consistent with the type of the geosynthetic. The reasons for this result are: (1) different mechanisms (e.g., separation, lateral restraint, and tensioned membrane) occurred in the test sections with geosynthetics, and (2) although construction was carefully controlled, subtle variations in subgrade and base properties still existed among these test sections. For example, the test section with a GG/NW (i.e., GG over NW) composite had the greatest deformation among all the sections with geosynthetic in the VGB sections but the test section with the same GG/NW combined had the least deformation among the sections with geosynthetic in the RCA sections. The section with the GG/NW composite had the most deformation among all the sections with

geosynthetic in the VGB sections because the subgrade in this section had the lowest CBR value. In addition, there was a lack of interaction between the subgrade and the granular base as evidenced by no aggregate imprint on the surface of the subgrade in this test section during excavation. Aggregate imprints were visually seen on the surface of the subgrade in other sections with geosynthetic during excavation. No aggregate imprint might indicate insufficient compaction close to the interface between the subgrade and the base for this test section. Table 3.2 clearly shows that both geosynthetic stabilization and use of RCA are effective at limiting permanent deformations.

Table 3.2: Accumulated Permanent Deformations of Unpaved Road Sections up to Load Sequence 9

Base Course	Geosynthetic	Subgrade CBR (%)	Accumulated Permanent Deformation (mm)
VGB	Control	1.9	32.43
VGB	NW	2.2	13.48
VGB	W	2.2	14.80
VGB	GG	2.1	14.16
VGB	GG/NW	1.9	24.48
RCA	Control	2.1	10.28
RCA	NW	2.0	6.71
RCA	W	2.0	8.22
RCA	GG	2.0	8.87
RCA	GG/NW	2.0	5.65

Figure 3.3 shows the resilient deformation for each test section after each unload. Most test sections show similar linear relationships except for the test section with VGB and woven geotextile. This consistent trend is in contrast to the different permanent deformation trends shown above. The test section with VGB and woven geotextile showing a different resilient behavior may be explained by a larger permanent deformation resulting in a tensioned membrane effect inducing more rebound of the test section during unloading. In typical mechanistic-empirical design, permanent deformation of a pavement is correlated to its resilient deformation, but this is not the case when a geosynthetic is placed at the interface between base course and subgrade. Sun et al.

(2017a) provided explanations for this phenomenon and suggested a method to back-calculate resilient modulus of a base course stabilized by a geosynthetic. This method was used to back-calculate resilient moduli of the test sections in the current study and will be presented later.

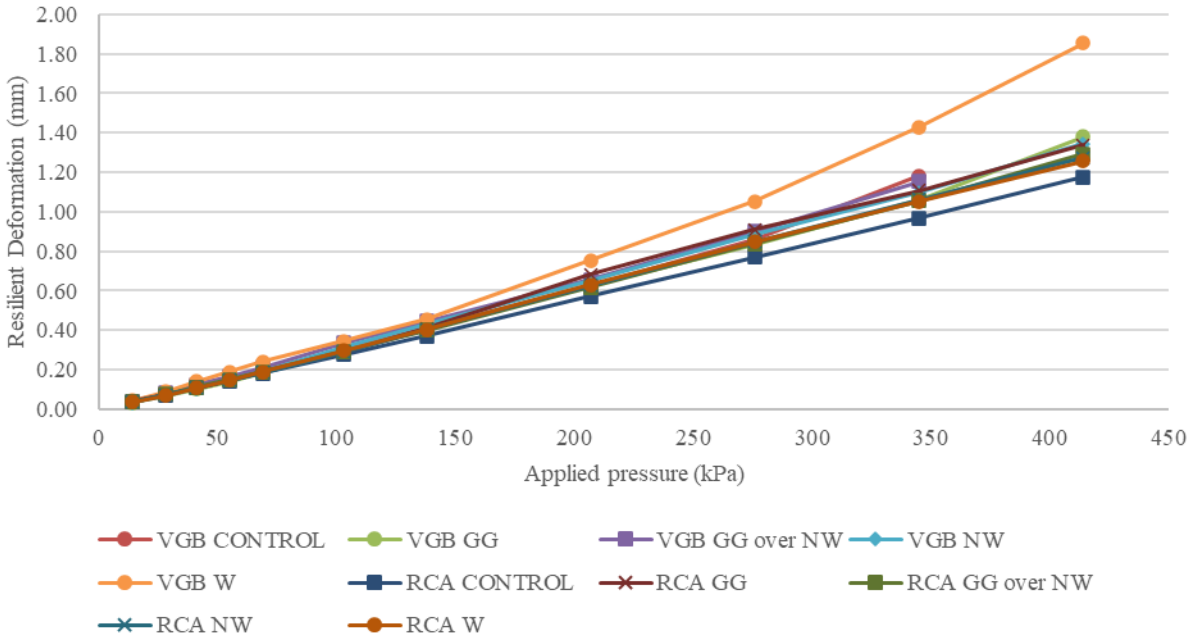

Figure 3.3: Average Resilient Deformations of Unpaved Road Sections by Load Sequence

3.4 Vertical Interface Stress

Earth pressure cells placed at the interface of the subgrade and the base course (or geosynthetic) measured the vertical stresses from surface loading in the unpaved road sections. Figure 3.4 shows the vertical interface stress normalized to the applied surface pressure ($\Delta\sigma/p$) versus the load cycle for each test section. The lower interface stress indicated more surface pressure distribution through the base course layer, which can be quantified by a stress distribution angle as discussed in Chapter 1. Figure 3.5 shows the stress distribution angles estimated from the measured vertical interface stresses at the center of the interface between the base and the subgrade. A higher distribution angle indicates a lower interface stress as the base course section spreads a load over a wider area at depth. The VGB sections display an increase in the normalized stresses in later stages when $\Delta\sigma/p$ became larger. The geogrid-stabilized VGB section exhibits the most consistent normalized interface stress and thus indicates a stable base course section. Although the

nonwoven-stabilized VGB section exhibits smaller permanent deformations over the load sequence, the interface stress increases at later stages indicate that at the larger loads the section was more prone to failure than the geogrid-stabilized VGB section. The normalized interface stresses for all RCA sections generally decreased with the number of cycles and the increased load magnitudes.

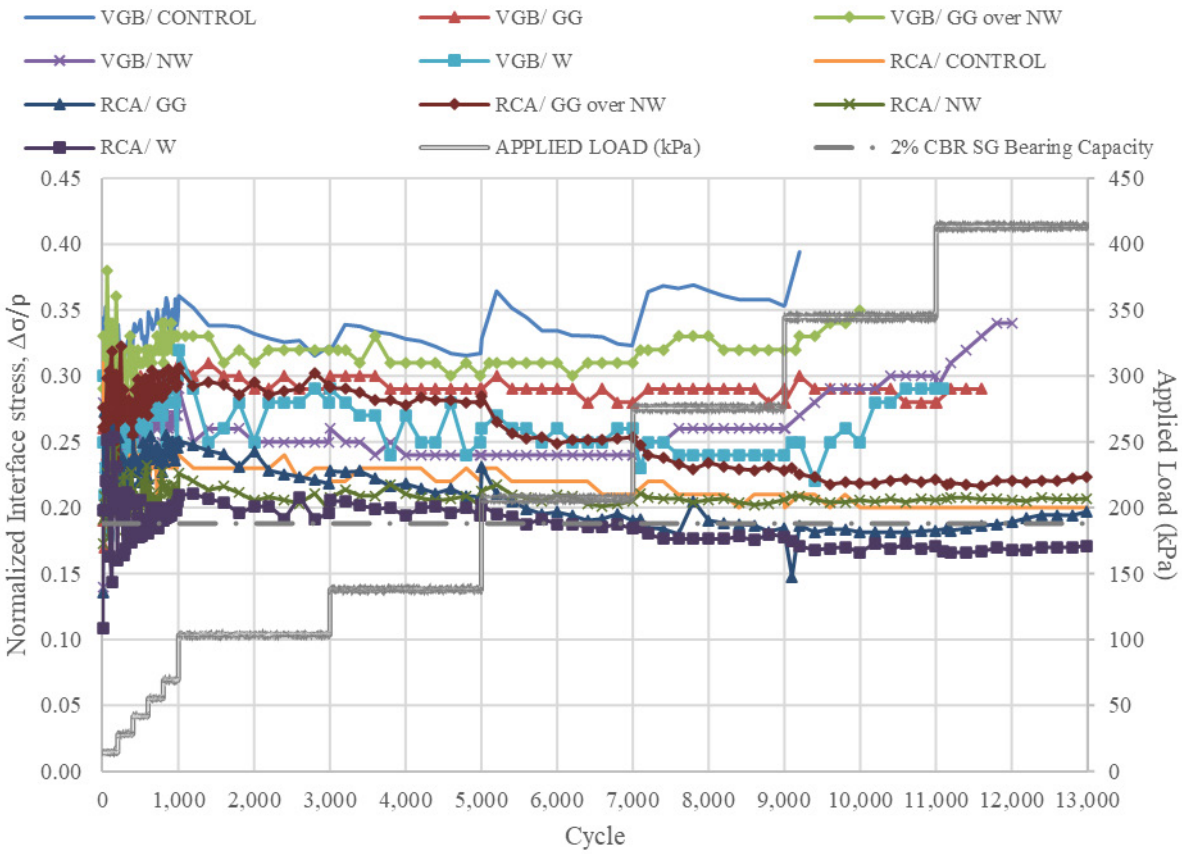

Figure 3.4: Normalized Interface Stresses in Unpaved Road Sections

Figure 3.5 shows the stress distribution angle for each test section at the end of each load increment. Figure 3.5 shows that the distribution angles for the RCA sections increased in the later load stages. However, the VGB sections show some increase in the distribution angle from Load Stage 5 to Load Stage 8 and then started to decrease. Overall, the RCA sections had larger distribution angles than the VGB sections so that the interface stresses and the permanent deformations decreased. The use of geosynthetic increased the distribution angle. The combination of the RCA base and the geosynthetic resulted in larger distribution angles. However, the relative

comparisons among the distribution angles for different geosynthetics are not necessarily correlated to those among the permanent deformations for the corresponding geosynthetics because of different mechanisms and material property variations involved.

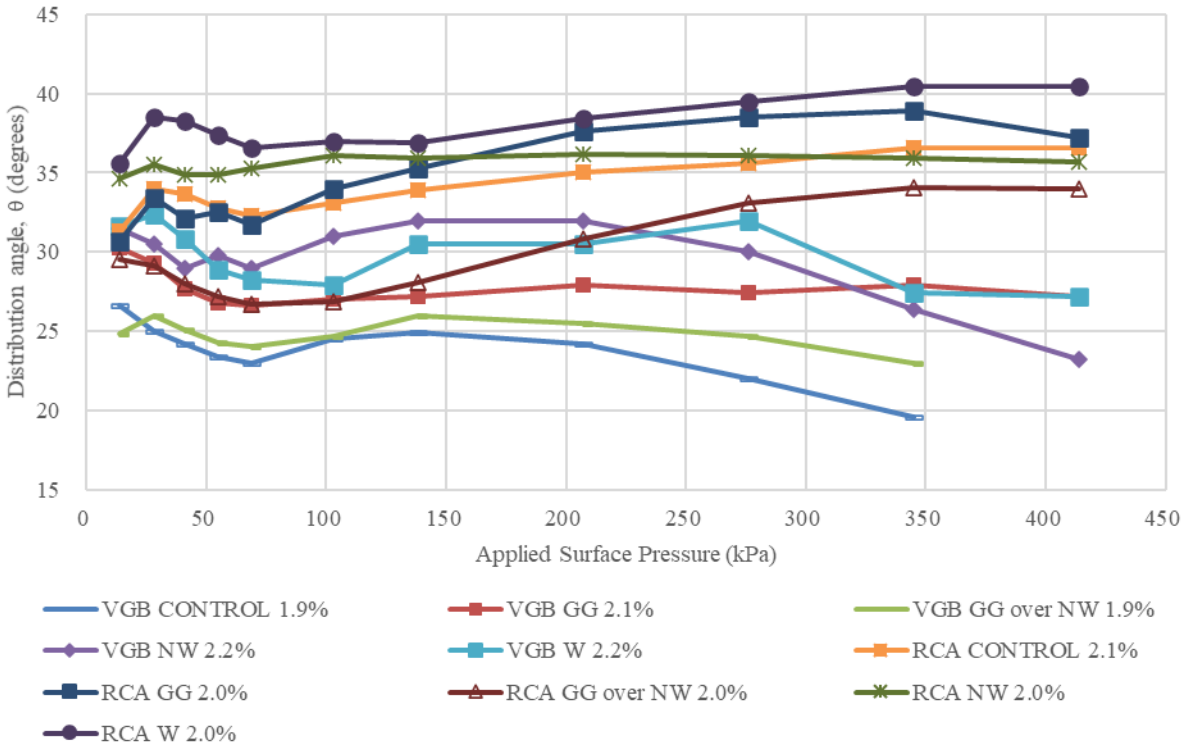

Figure 3.5: Stress Distribution Angle from Interface Stress in Unpaved Road Sections

3.5 Resilient and Subgrade Reaction Moduli

Figure 3.6 shows the average calculated resilient moduli of the base course sections for the 2,000-cycle load sequences determined by two different methods as compared with the accumulated permanent deformations after 9,000 cycles. As discussed in Chapter 1, the modified Burmister continuity equations (noted as "Burmister (MATLAB)" in Figure 3.6) proposed by Sun et al. (2017a) related the decreased permanent deformation to the increased resilient modulus. The stress reduction method (noted as "Stress Reduction" in Figure 3.6) resulted in variable values but it did show the benefits of using geosynthetic as well as the replacement of virgin aggregates with RCA. Sun et al. (2017a) concluded that the resilient modulus back-calculated based on the accumulated permanent deformation is more reliable than that based on the vertical interface

stress. Between these two methods, the modified Burmister method by Sun et al. (2017a) back-calculated the resilient moduli correlated better with the accumulated permanent deformation after 9,000 load cycles than the stress reduction method; therefore, the modified Burmister method is recommended for future use.

For concrete pavement design, the modulus of subgrade reaction (k-value) of a base over a subgrade is required as discussed in Chapter 1. AASHTO (1993) provided a design chart to convert the combined effect of the resilient modulus of subgrade and the modulus of the base into the modulus of subgrade reaction (k-value) using Figure 1.8. Based on the test sections with 2% CBR subgrade (i.e., resilient modulus, M_r = 3,000 psi) and 250 mm (10 in.) base course, the relationship between the composite modulus of subgrade reaction thickness taken from Figure 1.8 (AASHTO, 1993) yields Equation 3.1.

$$\boldsymbol{k\,(pci) = 59\ln\left(M_{r,Base}\right) - 347} \qquad \textbf{Equation 3.1}$$

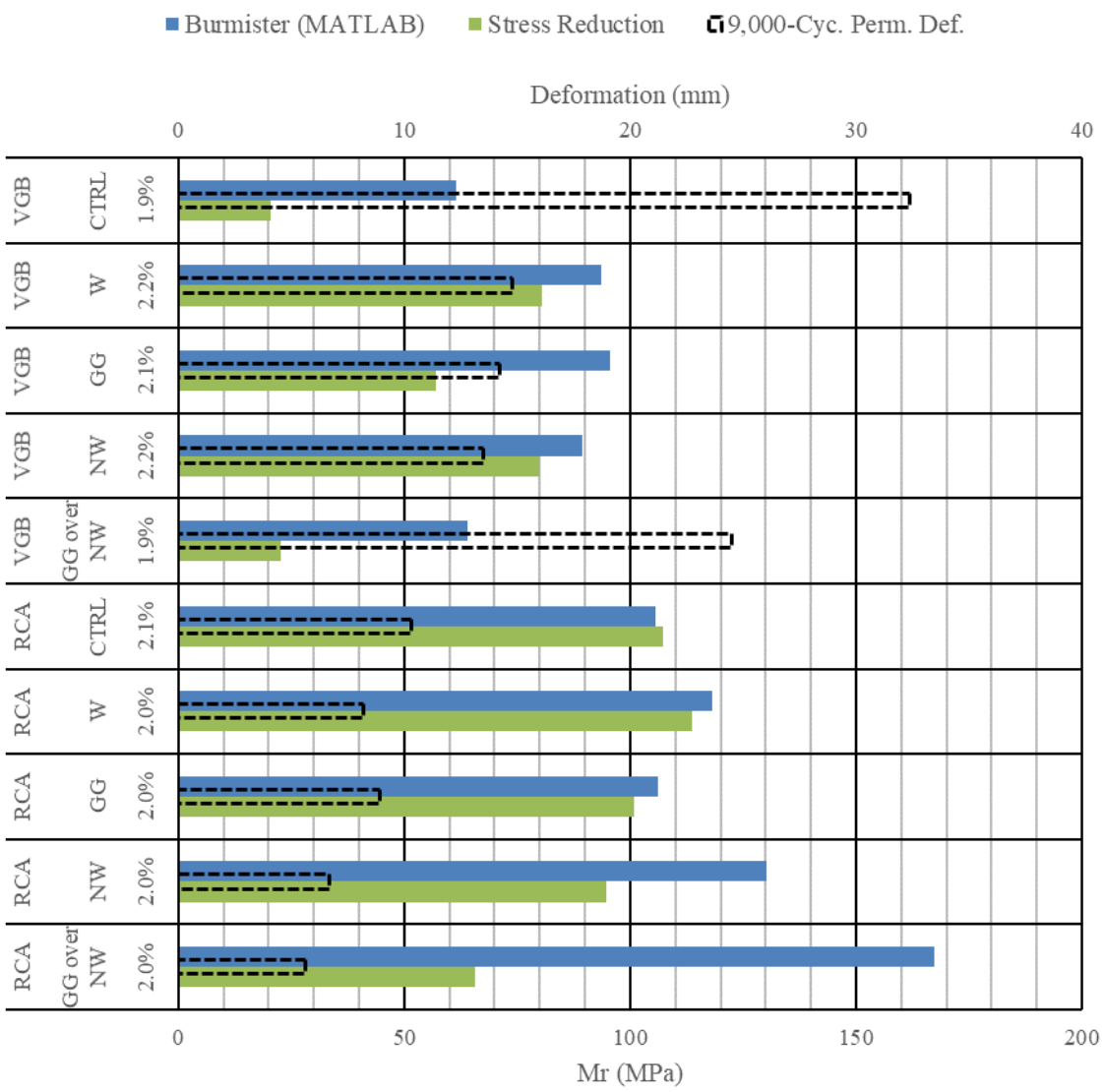

Figure 3.6: Average Back-Calculated Resilient Moduli of Unpaved Base Courses Using the Test Data following 2,000-Cycle Sequences

The back-calculated resilient moduli of the bases in Figure 3.6 were used to estimate the k-values using Equation 3.1 and Figure 1.8 and are plotted in Figure 3.7. Since the modified Burmister method better correlates the resilient moduli of the base courses to the permanent deformations of the test sections, it is the preferred method to estimate the k-values, which range from 51 to 67 Mpa/m (188 to 247 pci). Typical k-values for non-stabilized virgin granular base range from 13.5 to 270 Mpa/m (50 to 994 pci) (AASHTO, 1993); therefore, the k-values

determined by the modified Burmister method and the AASHTO chart are reasonable. In addition, these values are close to the upper limit reported by Westergaard (1926).

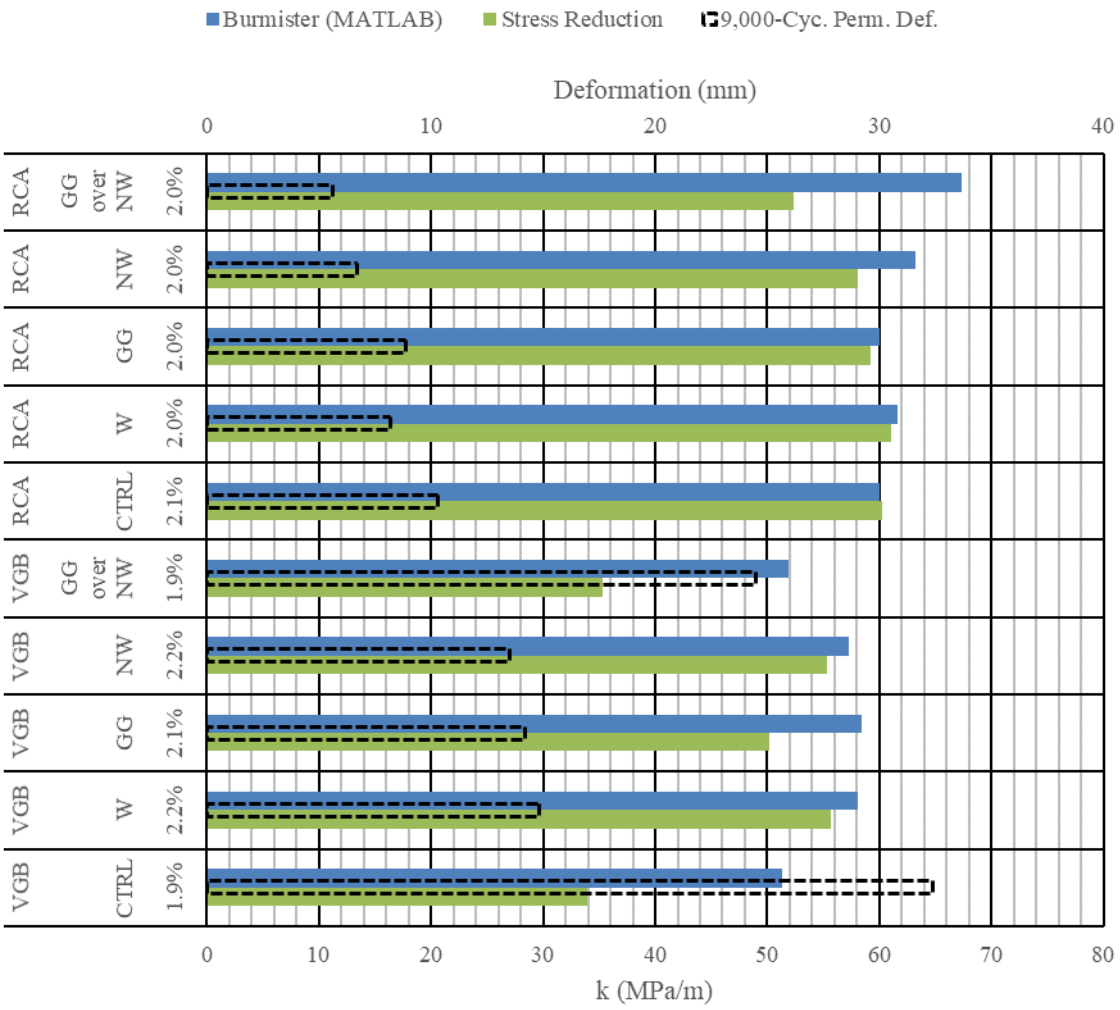

Figure 3.7: Modulus of Subgrade Reaction Using Two Methods for Unpaved Road Sections from Subgrade and Base Resilient Moduli and Figure 1.8

To evaluate the improvement of the resilient moduli, M_r, and the moduli of subgrade reaction, k, of the granular bases stabilized by different geosynthetics, the following improvement factors are defined by Equation 3.2 and Equation 3.3.

$$I_{f,M} = \frac{M_{r,s}}{M_{r,c}}$$ **Equation 3.2**

$$I_{f,k} = \frac{k_s}{k_c}$$ **Equation 3.3**

Where:

$I_{f,M}$ = the improvement factor for the resilient modulus of the stabilized base,

$I_{f,k}$ = the improvement factor for the modulus of subgrade reaction of the stabilized base,

$M_{r,s}$ and $M_{r,c}$ = the resilient moduli of the stabilized and control bases, respectively; and

$k_{r,s}$ and $k_{r,c}$ = the resilient moduli of the stabilized and control bases, respectively.

Table 3.3 provides the calculated improvement factors for the resilient moduli of the granular bases stabilized by the geosynthetics while Table 3.4 provides the calculated improvement factors for the moduli of subgrade reaction of the granular bases stabilized by the geosynthetics over the subgrade soil. Table 3.3 shows that the improvement factors for the M_r values of the geosynthetic-stabilized bases back-calculated by the modified Burmister method range from 1.01 to 1.58, which are in agreement with the recommendation by Han (2015) and correlated well with the accumulated permanent deformations. However, the improvement factors for the M_r values calculated by the stress reduction method ranged from 0.61 to 3.94, which are not that reasonable as back-calculated by the modified Burmister method. Table 3.4 shows that the improvement factors for the k-values calculated using the base M_r values back-calculated by the modified Burmister method range from 1.00 to 1.14. However, the improvement factors for the k-values calculated using the base resilient moduli back-calculated by the stress reduction method range from 0.87 to 1.64, which are more variable and not correlated well with the accumulated permanent deformations. The improvement factors for the k-values of the test sections are much less than those for the base M_r values because the k-values include the contributions by both the base and the subgrade while the subgrade M_r values were approximately the same between the control and stabilized sections.

Table 3.3: Improvement Factors for Resilient Moduli of Unpaved Bases

Base Course	Geosynthetic	Burmister, M_r (Mpa)	$I_{f, M}$	Stress Reduction, M_r (Mpa)	$I_{f, M}$
VGB	Control	61.1	-	20.4	-
VGB	W	93.5	1.53	80.4	3.94
VGB	GG	95.6	1.56	56.9	2.79
VGB	NW	89.5	1.46	79.8	3.91
VGB	GG/NW	64.0	1.05	24.5	1.20
RCA	Control	105.6	-	107.4	-
RCA	W	118.1	1.12	113.7	1.06
RCA	GG	106.3	1.01	101.0	0.94
RCA	NW	130.1	1.23	94.6	0.88
RCA	GG/NW	167.1	1.58	65.8	0.61

Note: 1 Mpa = 145 psi.

Table 3.4: Improvement Factors for Moduli of Subgrade Reaction of Unpaved Sections

Base Course	Geosynthetic	Mod. Burmister k (Mpa/m)	$I_{f, k}$	Stress Reduction k (Mpa/m)	$I_{f, k}$
VGB	Control	51.3	-	33.9	-
VGB	W	58.1	1.13	55.6	1.64
VGB	GG	58.4	1.14	50.2	1.48
VGB	NW	57.3	1.12	55.4	1.63
VGB	GG/NW	51.8	1.01	35.3	1.04
RCA	Control	60.0	-	60.3	-
RCA	W	61.6	1.03	61.1	1.01
RCA	GG	60.0	1.00	59.2	0.98
RCA	NW	63.2	1.05	58.1	0.96
RCA	GG/NW	67.3	1.12	52.4	0.87

Note: 1 Mpa/m = 3.7 pci

Figure 3.8 shows the back-calculated k-values of the test sections are plotted against the 9,000-cycle permanent deformations and the stress distribution angle. The modified Burmister method incorporated in MATLAB resulted in a better correlation between the k-value and the permanent deformation while the stress reduction method resulted in a better correction between the k-value and the stress distribution angle. Figure 3.8 also shows that the small increase of the k-value from 51 Mpa/m or 189 pci to 67 Mpa/m or 248 pci (31% increase) resulted in the reduction of the accumulated permanent deformation from 32.4 mm or 1.3 in. to 5.6 mm or 0.2 in. (83% reduction).

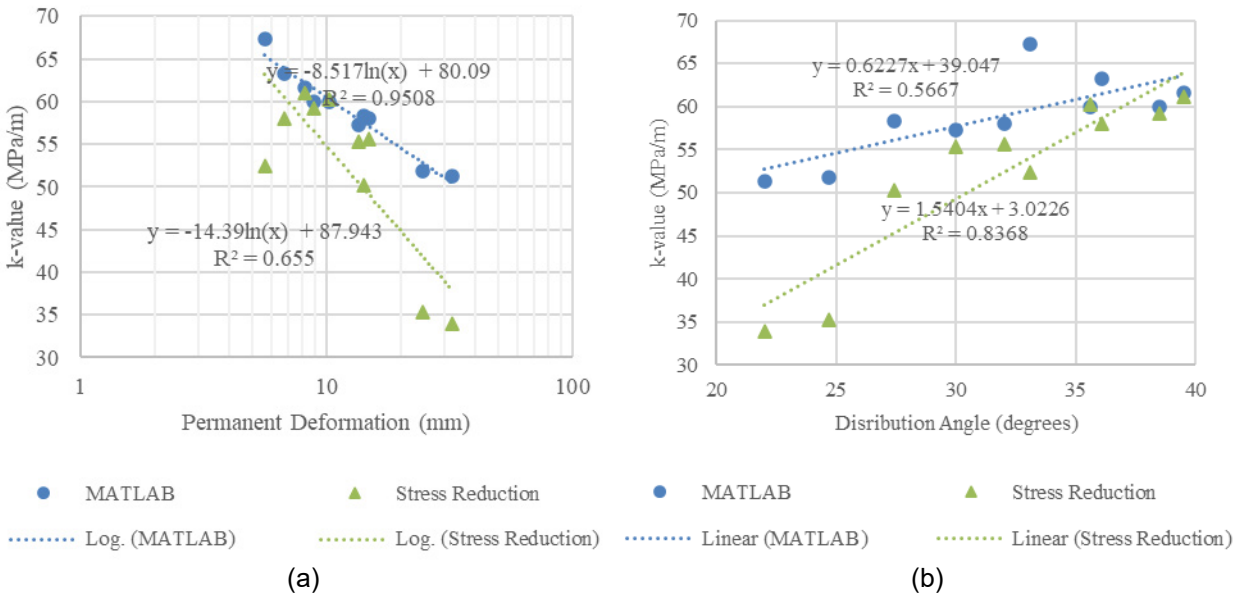

Figure 3.8: Moduli of Subgrade Reaction of Unpaved Sections vs.: (a) Permanent Deformation and (b) Distribution Angle

Benefits in the improved performance (e.g., reduced permanent deformation and increased distribution angle) and the estimated M_r and k-values of unpaved sections were observed by the addition of geosynthetic as well as the replacement of VGB with RCA. Based on the unpaved test results, the greatest improvement in the k-values occurred due to the replacement of VGB with RCA, which improves the section k-value by more than 25% on average. The addition of a geosynthetic further improved the k-value by an average of 10% in the VGB and an average of 5% in the RCA. Geosynthetics reduced the permanent deformations by more than 45% in the VGB and 25% in the RCA, and RCA replacement reduced the permanent deformation of a section by more than 55% when compared with VGB. Overall, a greater improvement from the VGB control section is observed through RCA replacement than through the addition of a geosynthetic, but even in the stronger granular base sections, further improvement to the unpaved section performance was observed through the addition of a geosynthetic. Considering good overall performance, unique functions of separation, filtration, and drainage, and low cost, the non-woven geotextile was selected for further studies in concrete pavements to be discussed in next chapter.

Chapter 4: Concrete Pavement Test Results and Analysis

4.1 Introduction

After understanding the behavior and estimating the properties of unpaved road sections with different granular bases and geosynthetics under cyclic loading, behavior and properties of concrete paved road sections with the same granular bases and the selected non-woven geotextile were evaluated and are presented in this chapter.

4.2 Displacement of Concrete Pavement

To verify the benefit of RCA as compared with VGB and the further benefit due to the stabilization of geosynthetic (non-woven geotextile) in concrete pavements, three concrete pavement sections were constructed in the large box and loaded cyclically after curing of each pavement section and again after one simulated rainfall event. It should be noted that unlike the loading sequence of different load increments for unpaved road tests, a constant load magnitude of 9 kips (40 kN) was used for cyclic loading on concrete pavements, which is better to simulate traffic loading in the practice. Figure 4.1 shows the actuator displacements at the corner loaded by the actuator through the loading plate. Since the applied load on the concrete pavement was larger than that on the unpaved section, the resilient displacement appears to be larger than that in the unpaved road test. However, the trend for permanent deformations is consistent with that in the unpaved road tests. The nonwoven geotextile and furthermore the RCA replacement reduced the permanent deformations under the given load sequence. Figure 4.1 clearly shows that rainfall increased the total and permanent deformations of all three test sections, especially right after the rainfall. However, the rate of deformation decreased with the number of load cycles. It is expected that without the rainfall, the total and permanent deformations would continue increasing with a small deformation rate. The differences between the actual deformations and the expected deformations without the rainfall are the additional deformations due to the rainfall. This comparison indicates the rainfall had a detrimental effect on the concrete pavement performance.

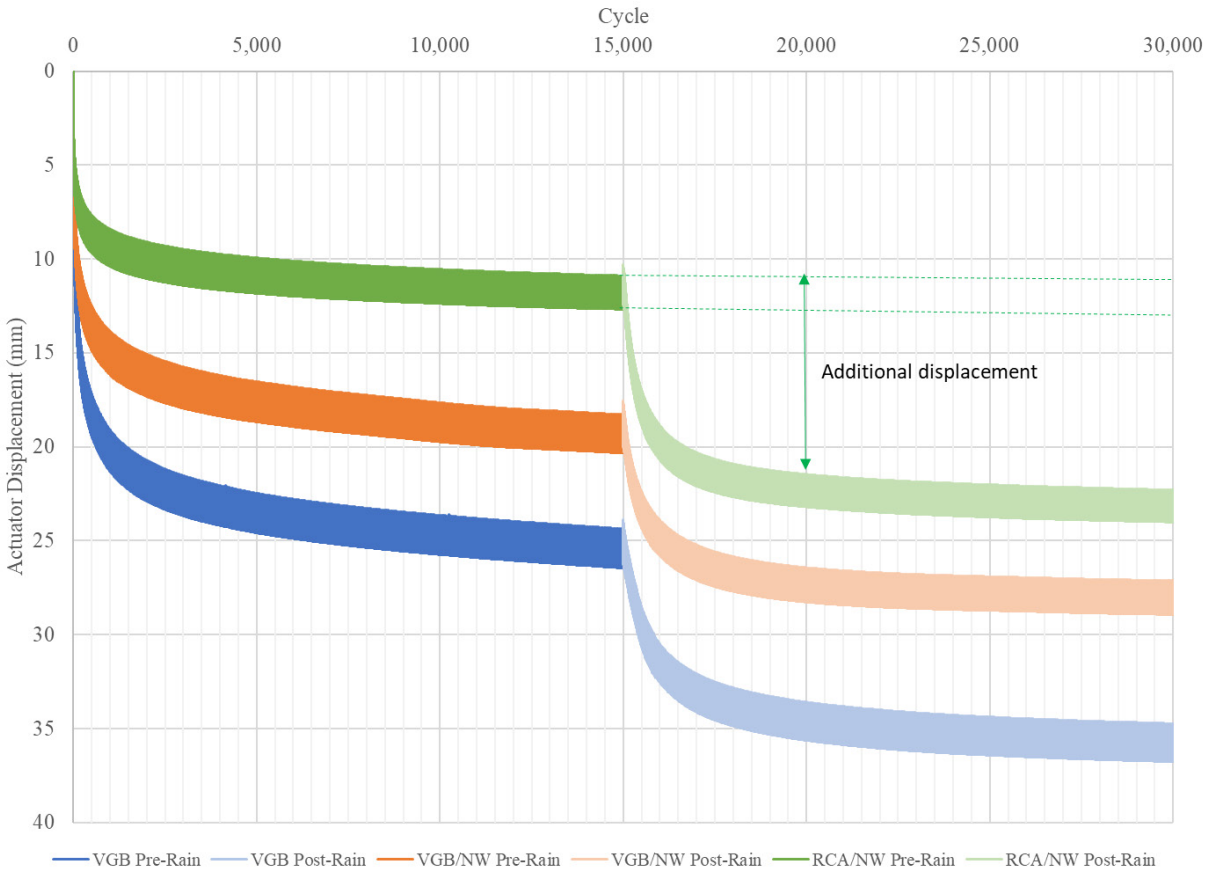

Figure 4.1: Actuator Displacements vs. Load Cycles for Concrete Pavement Sections

Figure 4.2 and Figure 4.3 show the permanent deformations of the concrete pavements under cyclic loading before rainfall and the additional permanent deformations after rainfall. Please note different vertical scales are used in these two figures to help display the data in Figure 4.3. During the first test on the VGB section, no displacement transducer was placed at the corner of the concrete slab initially and then added after 4,000 load cycles. Therefore, the initial portion of the curve was estimated based on the measured displacements on the loading plate and at two other locations. It is clearly shown that the VGB section had the largest permanent deformation, which was reduced by the use of the non-woven geotextile and further reduced by the replacement with RCA. The rainfall had a similar detrimental effect on the permanent deformations of concrete pavements with or without geotextile as shown in Figure 4.3.

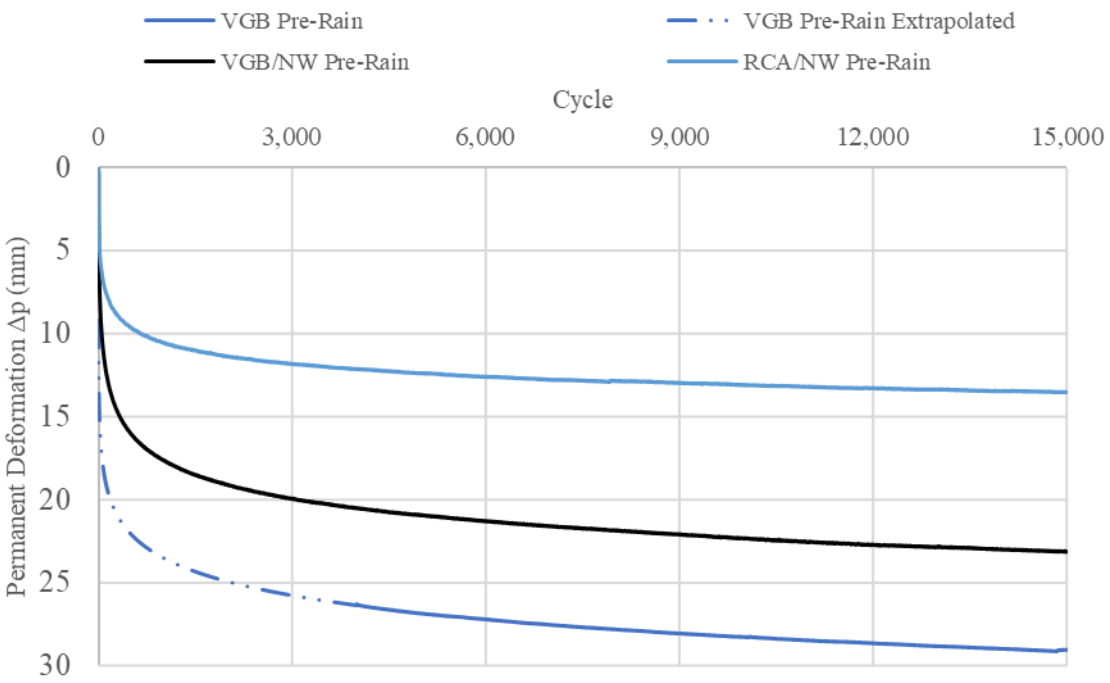

Figure 4.2: Corner Displacements for Concrete Pavements before Rainfall

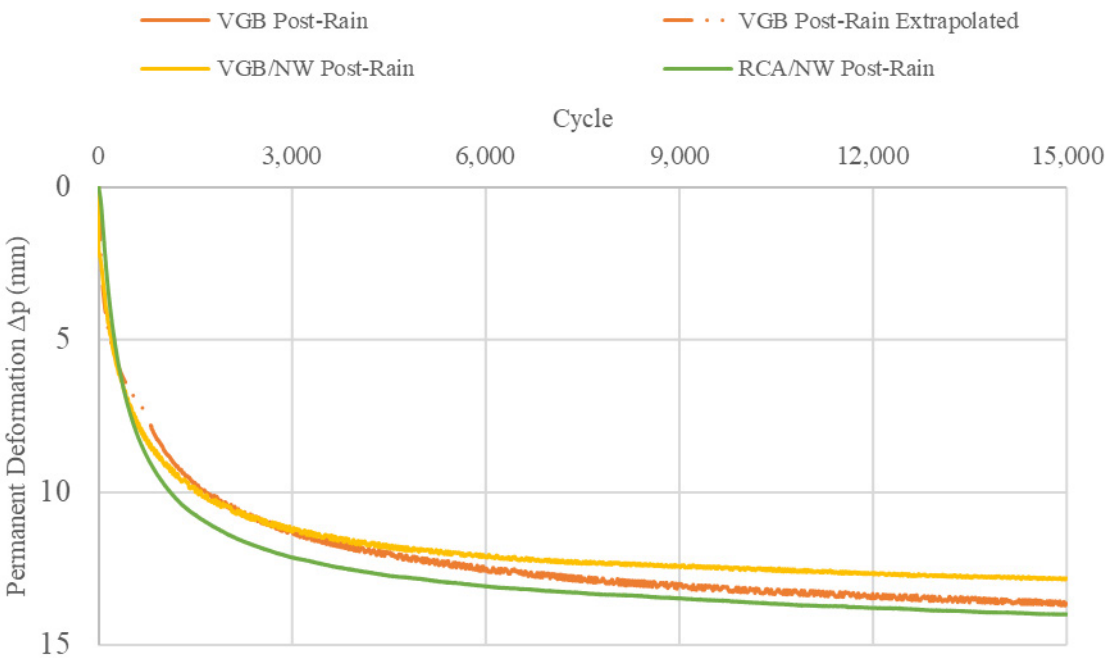

Figure 4.3: Corner Displacements for Concrete Pavements after Rainfall

4.3 Modulus of Subgrade Reaction

The maximum displacement at the corner for each load application combined with the displacements taken at twice and thrice the radius along the diagonal of the loaded slab allow for determining the distance of the rotation of the concrete slab to the center of the load, L, as shown in Figure 2.26. Considering the definition of the radius of relative stiffness as a radius of gyration by Westergaard (1926), the finite slab dimension, and the resisting post placed at the farther corner in this study, the distance from the center of the load to the estimated point of slab rotation, L, was assumed equal to the radius of relative stiffness, *l*, which was used in Equation 1.2 to estimate the modulus of subgrade reaction (k-value) based on Westergaard's (1926) solution. Figure 4.3 shows that the subgrade reaction moduli increase with the number of applied load cycles before rainfall, indicating that the base course sections were compressed under cyclic loading until the subgrade reaction became consistent in the last 12,000 cycles. For a reference, the lower and upper limits of the k-values in Westergaard (1926) from static loading of non-stabilized base courses are plotted. The k-values for the VGB control section are between the lower and upper limits in Westergaard (1926). The k-values for the VGB/NW section are close to the upper limit while the k-values for the RCA/NW section are above the upper limit. The k-values from the unpaved road tests shown in Table 3.4. are 51.3 PMa/m or 190 pci (VGB control), 57.3 MPa/m or 212 pci (VGB/NW), and 63.2 MPa/m or 234 pci (RCA/NW), which are close to those k-values of 45.8 MPa/m or 169 pci (VGB), 54.3 MPa/m or 201 pci (VGB/NW), and 68.9 MPa/m or 255 pci (RCA/NW) found in the concrete pavement tests before rainfall as shown in Figure 4.3. This comparison demonstrates that the k-values determined from the unpaved test sections can be used to predict the performance of concrete pavements on the same base and subgrade with or without a geosynthetic. Geosynthetic stabilization and RCA replacement of VGB increased the k-values of the test sections.

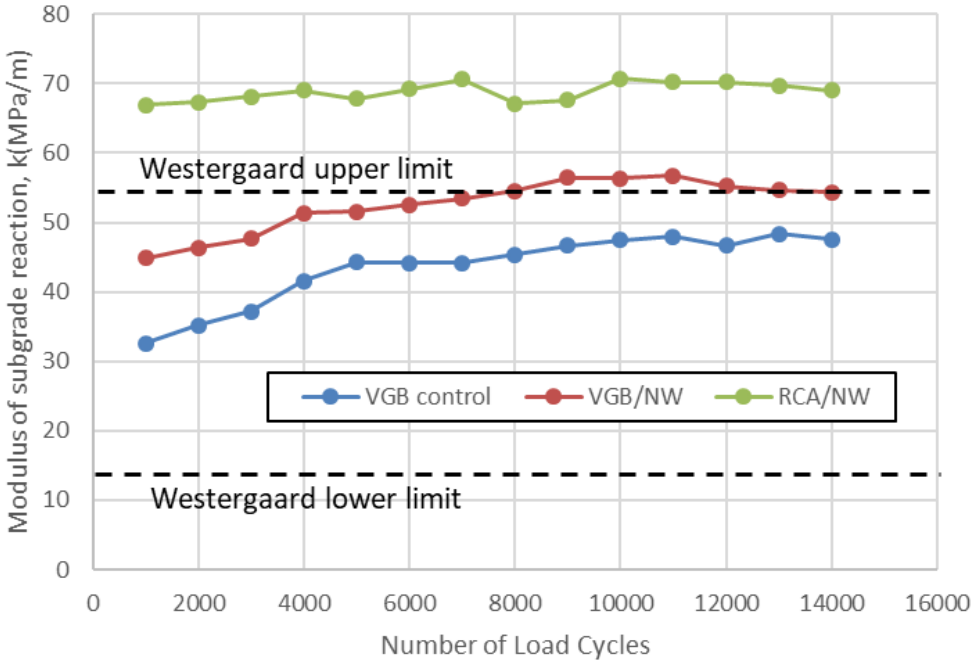

Figure 4.4: Moduli of Subgrade Reaction (k-value) for Different Concrete Pavement Sections versus Number of Load Cycles before Rainfall

Figure 4.5 shows the moduli of subgrade reaction (k-values) at the end of cyclic loading as compared with the permanent deformations at the corresponding load. It is clearly shown that the test section with a higher subgrade reaction modulus resulted in a smaller permanent deformation. The nonwoven geotextile increased the k-value in the VGB section by 17%. Replacement of VGB with RCA in the nonwoven-stabilized sections increased the k-value by 27%. The percent of the increase for the k-value in the concrete pavement by the non-woven geotextile is similar to that in the unpaved road. However, the percent of the increase for the k-value in the concrete pavement by the replacement of VGB with RCA is more than that in the unpaved road.

Figure 4.6 shows the semi-logarithmic relationship between the modulus of subgrade reaction of the section and the accumulated permanent deformation at the end of cyclic loading before rainfall. Similar to the finding from the unpaved road tests, an increase of the modulus of subgrade reaction resulted in a reduction of the accumulated permanent deformation.

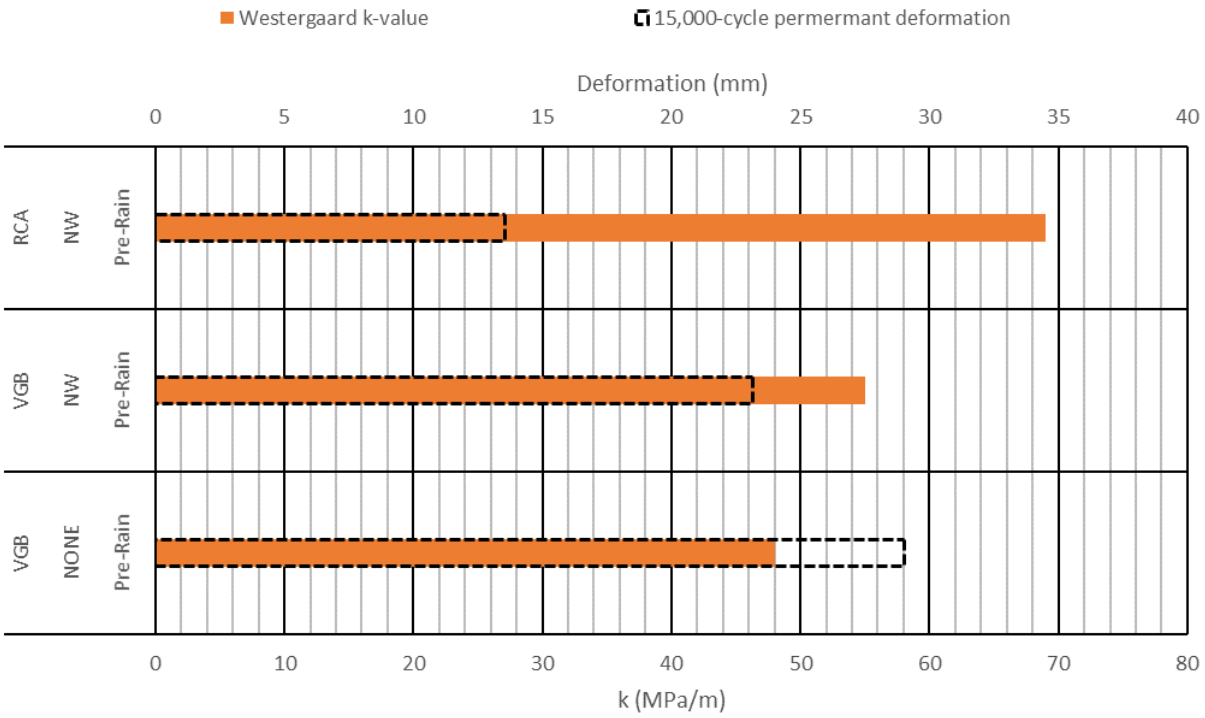

Figure 4.5: Modulus of Subgrade Reaction in Concrete Pavements at the End of Loading

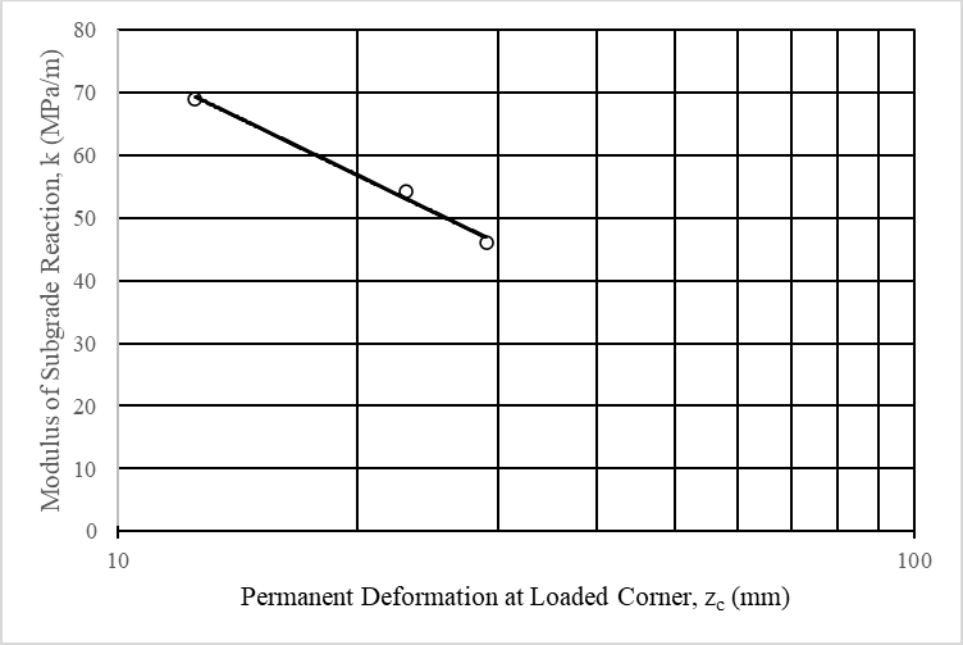

Figure 4.6: Permanent Deformation at the Loaded Corner of the Concrete Slab versus Modulus of Subgrade Reaction before Rainfall

Figure 4.7 shows the calculated tensile stresses in the concrete slab using the Westergaard (1926) solution (i.e., Equation 1.3). These calculated stresses are well below the tensile strength of the concrete slab based on UC testing as discussed earlier, and there was no cracking observed in the slabs upon extraction. Therefore, the concrete slab deformations were mostly contributed by the deformations of the base course or subgrade and not by the cracking of the slab.

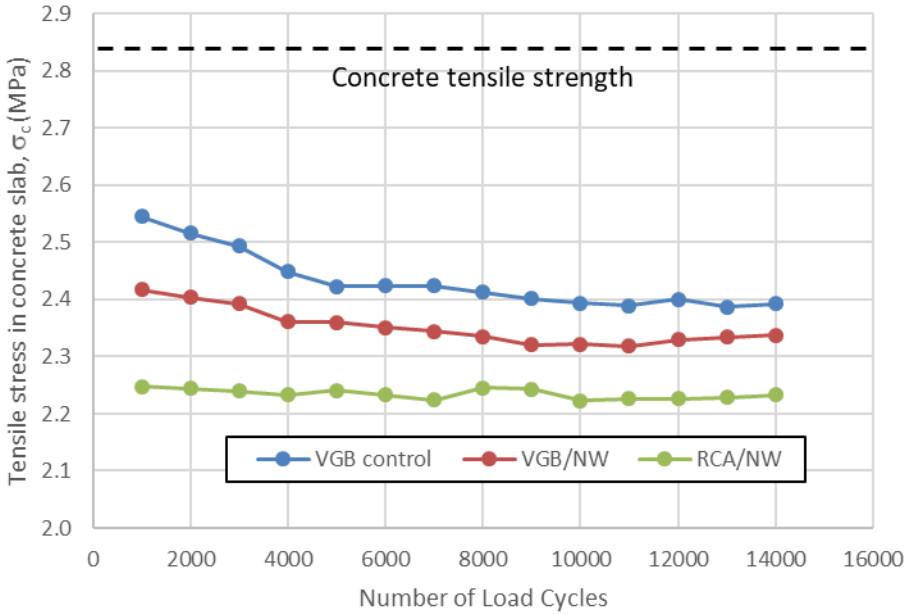

Figure 4.7: Calculated Tensile Stresses in the Concrete Slab due to Corner Loading before Rainfall using the Westergaard Solution

4.4 Interface Stress

The applied load on the concrete slab was distributed through the base course to the surface of the subgrade. The vertical stresses at the interface between the base and the subgrade were measured by earth pressure cells under the corner beneath the loaded concrete slab. Figure 4.8 shows the measured interface stresses for the concrete pavement tests with the number of load cycles. The ratios of the interface stress to the applied pressure on the concrete slab by the loading plate are lower than those observed in the unpaved road tests, as would be expected despite the increased applied pressure to 550 kPa (80 psi). Since the concrete slab distributes the applied load in a different way from the unpaved road, the normalized interface stresses have an opposite trend

than the displacements and the calculated k-values, which differ from those for the unpaved roads. For example, the nonwoven-geotextile-stabilized RCA had the smallest displacement but the highest normalized interface stress and the highest k-value. This result is reasonable because the stiffer subgrade reaction provided more support and attracted more interface stresses.

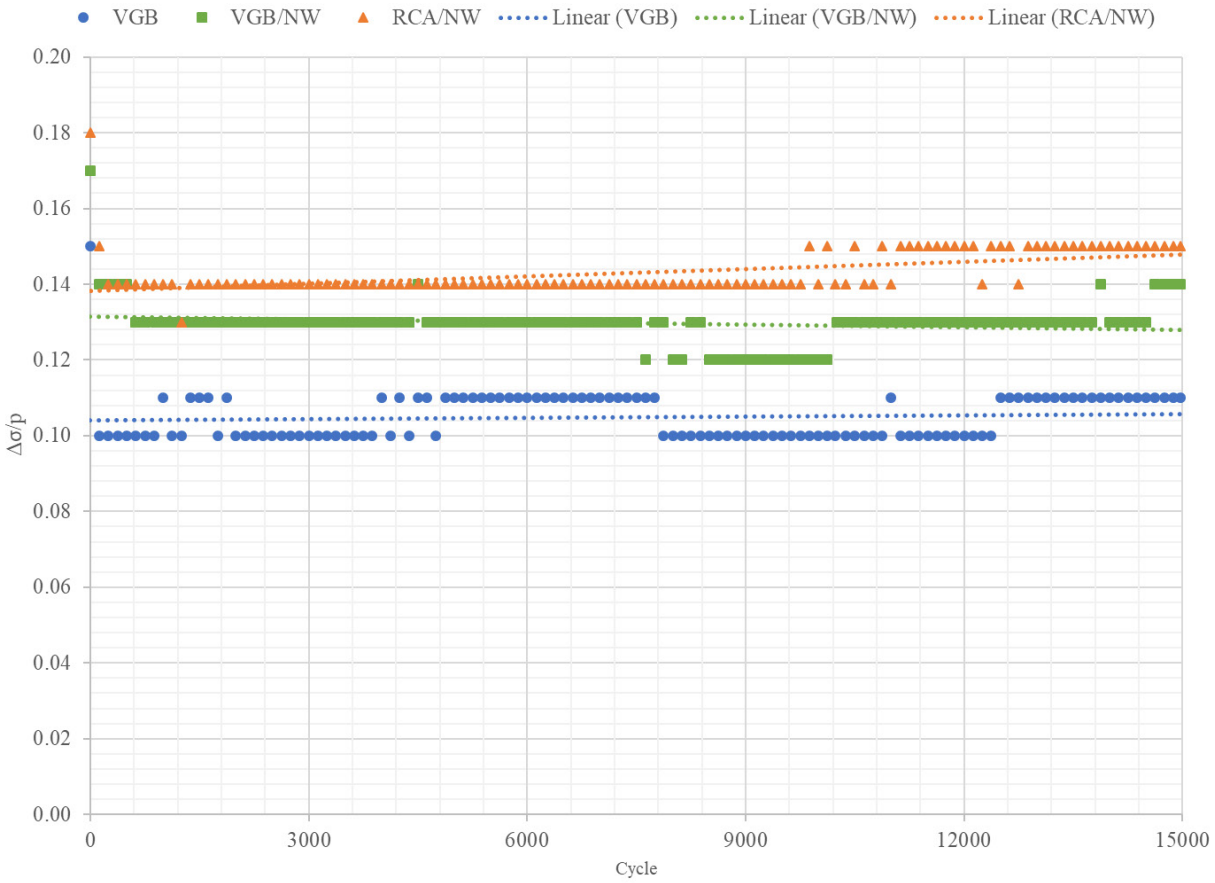

Figure 4.8: Measured Interface Stress Ratios at the Base Course-Subgrade Interface from Corner Loading on Concrete Pavements

Chapter 5: Conclusions

This study evaluated the options of using recycled aggregate with or without a geosynthetic to replace virgin granular aggregate as a base course for concrete pavements. A series of cyclic plate loading tests were conducted in a large test box on unpaved road sections and concrete pavement sections over weak subgrade. This study focused on the comparison between Virgin Granular Base (VGB) and Recycled Concrete Aggregate (RCA). Three different types of geosynthetics (nonwoven geotextile, woven geotextile, and triaxial geogrid) on the KDOT pre-qualified list were adopted in the unpaved road tests. During the tests, surface displacements and earth pressures at the interface between base and subgrade were monitored by displacement transducers and earth pressure cells. The modified Burmister solution and the stress distribution method were adopted to back-calculate the resilient moduli of non-stabilized and geosynthetic-stabilized VGB and RCA in unpaved road tests based on the measured permanent deformations and the measured interface stresses under cyclic loading. The back-calculated resilient moduli of the base courses were used to estimate the subgrade reaction moduli of the non-stabilized and geosynthetic-stabilized base courses over the subgrade using the AASHTO (1993) method. Based on reduced permanent deformation, separation, filtration, and drainage functions, and economic considerations, nonwoven geotextile was selected for concrete pavement tests. The subgrade reaction moduli of the non-stabilized and nonwoven geotextile-stabilized base courses over the subgrade under concrete pavements were back-calculated using the Westergaard (1926) method based on the corner loading tests. The following findings and/or conclusions can be obtained from this study:

Recycled concrete aggregate (RCA) tested in this study was stronger and stiffer than the virgin granular base (VGB) aggregate; therefore, the test sections with the RCA base course had smaller total and permanent deformations in unpaved roads and concrete pavements.

Geosynthetics (nonwoven geotextile, woven geotextile, and triaxial geogrid) placed between the aggregate base course and weak subgrade worked under different mechanisms (separation, lateral restraint, and tensioned membrane). The benefits of geosynthetics in improving the performance (e.g., permanent deformation and stress reduction) of roads depended on the

combined effect of these mechanisms and the tolerable deformation. Based on the test conditions (e.g., relatively small deformations for concrete pavements) adopted in this study, the nonwoven geotextile performed favorably overall in the improved performance of unpaved road sections as compared with other geosynthetics.

1. The back-calculated resilient moduli of non-stabilized and geosynthetic-stabilized aggregate base course using the modified Burmister solution by Sun et al. (2017a) correlated better with the measured permanent deformations in unpaved roads than the stress reduction method based on the measured interface stresses between the base and the subgrade.
2. Following the AASHTO (1993) design chart, the back-calculated resilient moduli of non-stabilized and geosynthetic-stabilized aggregate bases using the modified Burmister solution by Sun et al. (2017a) were successfully used with the subgrade resilient moduli to estimate the composite subgrade reaction moduli of the bases over the subgrade.
3. The subgrade reaction moduli of non-stabilized and nonwoven geotextile-stabilized aggregate bases over weak subgrade back-calculated by the Westergaard (1926) method correlated well with the permanent deformations of the concrete pavements loaded at the corner.
4. The subgrade reaction moduli of non-stabilized and nonwoven geotextile-stabilized aggregate bases over weak subgrade back-calculated by the Westergaard (1926) method were similar to those estimated by the resilient moduli of the subgrade and the base following the AASHTO (1993) design chart.
5. The nonwoven geotextile increased the subgrade reaction moduli of the VGB sections by approximately 15% in both unpaved and concrete paved road tests. The replacement of VGB with RCA further increased the subgrade reaction modulus by 10% in the unpaved road test or 27% in the concrete paved road test.

6. The accumulated permanent deformation of an unpaved or concrete paved section increased with the reduction of the subgrade reaction modulus in a semi-logarithmic relationship.
7. Rainfall had a detrimental effect on the total and permanent deformations of concrete pavements on aggregate bases over soft subgrade. The nonwoven geotextile had a limited effect on the permanent deformation of concrete pavements after rainfall.
8. In this study, the replacement of VGB with RCA had more obvious benefits on the improved performance of unpaved roads and concrete pavements than the use of a geosynthetic.

It should be noted that this study has the following limitations:

1. The compactor used in the laboratory had lower compaction energy than that used in the field; therefore, the measured CBR values for the aggregate bases were lower than those in the field. This might result in lower base course resilient moduli and lower composite subgrade reaction moduli.
2. The RCA was tested under cyclic loading for at most 30,000 cycles (beneath concrete pavement). The possible degradation of this material under long-term loading was not evaluated.
3. The rainfall study for concrete pavements only included one event and lasted for 15,000 load cycles. This might not be sufficient to simulate the erosion effect on concrete pavements and the benefit of geosynthetics to minimize the erosion effect from repeated rainfalls and other environmental factors.

Due to the above limitations, field studies are required to verify the findings from this study.

References

AASHTO T 307-99. (2017). *Standard method of test for determining the resilient modulus of soils and aggregate materials*. Washington, DC: American Association of State Highway and Transportation Officials.

American Association of State Highway and Transportation Officials (AASHTO). (1986). *AASHTO guide for design of pavement structures*. Washington, DC: Author.

American Association of State Highway and Transportation Officials (AASHTO). (1993). *AASHTO guide for design of pavement structures*. Washington, DC: Author.

American Association of State Highway and Transportation Officials (AASHTO). (2015). *Mechanistic-empirical pavement design guide: A manual of practice*. Washington, DC: Author.

ASTM D421-85. (2007). *Standard practice for dry preparation of soil samples for particle-size analysis and determination of soil constants*. West Conshohocken, PA: ASTM International. doi: 10.1520/D0421-85R07, www.astm.org

ASTM D698-12e2. (2012). *Standard test methods for laboratory compaction characteristics of soil using standard effort (12 400 ft-lbf/ft3 (600 kN-m/m3))*. West Conshohocken, PA: ASTM International. doi: 10.1520/D0698-12E02, www.astm.org

ASTM D1140-17. (2017). *Standard test methods for determining the amount of material finer than 75-µm (No. 200) sieve in soils by washing*. West Conshohocken, PA: ASTM International. doi: 10.1520/D1140-17, www.astm.org

ASTM D1556 / D1556M-15e1. (2015). *Standard test method for density and unit weight of soil in place by sand-cone method*. West Conshohocken, PA: ASTM International. doi: 10.1520/D1556_D1556M-15E01, www.astm.org

ASTM D1883-16. (2016). *Standard test method for California Bearing Ratio (CBR) of laboratory-compacted soils*. West Conshohocken, PA: ASTM International. doi: 10.1520/D1883-16, www.astm.org

ASTM D2166 / D2166M-16. (2016). *Standard test method for unconfined compressive strength of cohesive soil*. West Conshohocken, PA: ASTM International. doi: 10.1520/D2166_D2166M-16, www.astm.org

ASTM D4318-10. (2010). *Standard test methods for liquid limit, plastic limit, and plasticity index of soils*. West Conshohocken, PA: ASTM International. doi: 10.1520/D4318-10, www.astm.org

ASTM D4648 / D4648M-16. (2016). *Standard test methods for laboratory miniature vane shear test for saturated fine-grained clayey soil*. West Conshohocken, PA: ASTM International. doi: 10.1520/D4648_D4648M-16, www.astm.org

ASTM D7380-08. (2008). *Standard test method for soil compaction determination at shallow depths using 5-lb (2.3 kg) dynamic cone penetrometer*. West Conshohocken, PA: ASTM International. doi: 10.1520/D7380-08, www.astm.org

Burmister, D. M. (1945). The general theory of stresses and displacements in layered (soil) systems. I, II, III. *Journal of Applied Physics, 16*, 89–94; 126–127; 296–302.

Burmister, D. M. (1958). Evaluation of pavement systems of the WASHO road test by layered system methods. *Highway Research Board Bulletin, 177*, 26–54.

Edgar Minerals. (2018). *EPK clay*. Retrieved from http://www.edgarminerals.com/EPK-Clay.html

Giroud, J. P., & Han, J. (2004a). Design method for geogrid-reinforced unpaved roads. I. Development of design method. *Journal of Geotechnical and Geoenvironmental Engineering, 130*(8), 775–786.

Giroud, J. P., & Han, J. (2004b). Design method for geogrid-reinforced unpaved roads. II. Calibration and applications. *Journal of Geotechnical and Geoenvironmental Engineering, 130*(8), 787–797.

Guo, J., Han, J., Schrock, S. D., Sun, X., & Parsons, R. L. (2016). *Stabilization of unpaved shoulders on moderate and weak subgrade using geosynthetics* (Report No. K-TRAN: KU-13-2). Topeka, KS: Kansas Department of Transportation.

Han, J. (2015). *Principles and practice of ground improvement*. Hoboken, NJ: John Wiley and Sons, Inc.

Han, J., & Thakur, J. K. (2015). Sustainable roadway construction using recycled aggregates with geosynthetics. *Sustainable Cities and Society, 14*, 342–350.

Huang, Y. H. (2004). *Pavement analysis and design* (2nd ed.). Upper Saddle River, NJ: Pearson Prentice Hall/Pearson Education, Inc.

Jung, Y., Zollinger, D. G., Cho, B. H., Won, M. & Wimsatt, A. J. (2012). *Subbase and subgrade performance investigation and design guidelines for concrete pavement* (Report No. FHWA/TX-12/0-6037-2). Austin, TX: Texas Department of Transportation.

Kansas Department of Transportation (KDOT). (2015). Section 1106: Aggregates for granular base. *Standard specifications for state road & bridge construction*. Topeka, KS: Author.

Kansas Department of Transportation (KDOT). (2018). *Index of prequalified materials and material sources, #48. Geotextile fabrics*. Retrieved from http://www.ksdot.org/burmatrres/pql/default.asp

MATLAB [Computer software]. MathWorks, Natick, MA.

Maxwell, S., Kim, W.-H., Edil, T. B., & Benson, C. H. (2005). *Effectiveness of geosynthetics in stabilizing soft subgrades* (Wisconsin Highway Research Program #0092-45-15). Madison, WI: Wisconsin Department of Transportation.

National Cooperative Highway Research Program (NCHRP). (2004). *Guide for mechanistic-empirical design of new and rehabilitated pavement structures* (NCHRP 1-37A). Washington, DC: Transportation Research Board.

Ober, J. A. (2017). Annual review 2016: Mining review. *Mining Engineering, 69*(5), 50–59.

Oluokun, F. A., Burdette, E. G., & Deatherage, J. H. (1991). Elastic modulus, Poisson's ratio, and compressive strength relationships at early ages. *ACI Materials Journal, 88*(1), 3–10.

Qian, Y., Han, J., Pokharel, S. K., & Parsons, R. L. (2011). Determination of resilient modulus of subgrade using cyclic plate loading tests. *Geo-Frontiers 2011: Advances in geotechnical engineering* (pp. 4743–4751). Reston, VA: ASCE.

Sun, X., Han, J., & Corey, R. (2017a). Equivalent modulus of geogrid-stabilized granular base back-calculated using permanent deformation. *Journal of Geotechnical and Geoenvironmental Engineering, 143*(9).

Sun, X., Han, J., Crippen, L., & Corey, R. (2017b). Back-calculation of resilient modulus and prediction of permanent deformation for fine-grained subgrade under cyclic loading. *Journal of Materials in Civil Engineering, 29*(5).

Sun, X., Han, J., Kwon, J., Parsons, R. L., & Wayne, M. H. (2015). Radial stresses and resilient deformations of geogrid-stabilized unpaved roads under cyclic plate loading tests. *Geotextiles and Geomembranes, 43*(5), 440–449.

Thakur, J. K., & Han, J. (2015). Recent development of recycled asphalt pavement (RAP) bases treated for roadway applications. *Transportation Infrastructure Geotechnology, 2*(2), 68–86.

Tseng, K.-H. (1988). *A finite element method for the performance analysis of flexible pavements* (Doctoral dissertation). Texas A&M University, College Station TX.

Tseng, K.-H., & Lytton, R. L. (1989). Prediction of permanent deformation in flexible pavement materials. In H. Schreuders & C. Marek (Eds.), *Implication of aggregates in the design, construction, and performance of flexible pavements* (ASTM STP 1016, pp. 154–172). West Conshohocken, PA: ASTM International.

Westergaard, H. M. (1926). Computation of stresses in concrete roads. Proceedings of the fifth annual meeting of the Highway Research Board held at Washington, D.C. December 3-4, 1925. Part I: Reports of research committees and of special investigations. *Highway Research Board Proceedings, 5*, 90–112.

K-TRAN

KANSAS TRANSPORTATION RESEARCH AND NEW-DEVELOPMENT PROGRAM

AD ASTRA PER ASPERA

Kansas

Department of Transportation